Received: 18 February 2022 | Revised: 26 April 2022 | Accepted: 12 May 2022

DOI: 10.1002/cne.25353

RESEARCH ARTICLE

JCN RESEARCH IN SYSTEMS NEUROSCIENCE THE JOURNAL OF COMPARATIVE NEUROLOGY WILEY

The brain of the tree pangolin (*Manis tricuspis*). VIII. The subpallial telencephalon

Aminu Imam[1,2] | **Adhil Bhagwandin**[1] | **Moyosore S. Ajao**[2] | **Paul R. Manger**[1]

[1]School of Anatomical Sciences, Faculty of Health Sciences, University of the Witwatersrand, Parktown, Johannesburg, Republic of South Africa

[2]Department of Anatomy, Faculty of Basic Medical Sciences, College of Health Sciences, University of Ilorin, Ilorin, Nigeria

Correspondence
Paul Manger, School of Anatomical Sciences, University of the Witwatersrand, 7 York Road, Parktown, Johannesburg 2193, Republic of South Africa.
Email: Paul.Manger@wits.ac.za

Associate Editor: Kathleen Rockland

Funding information
Third World Academy of Sciences; South African National Research Foundation

Abstract

The current study provides a detailed architectural analysis of the subpallial telencephalon of the tree pangolin. In the tree pangolin, the subpallial telencephalon was divided into septal and striatopallidal regions. The septal region contained the septal nuclear complex, diagonal band of Broca, and the bed nuclei of the stria terminalis. The striatopallidal region comprised of the dorsal (caudate, putamen, internal and external globus pallidus) and ventral (nucleus accumbens, olfactory tubercle, ventral pallidum, nucleus basalis, basal part of the substantia innominata, lateral stripe of the striatum, navicular nucleus, and the major island of Calleja) striatopallidal complexes. In the tree pangolin, the organization and numbers of nuclei forming these regions and complexes, their topographical relationships to each other, and the cyto-, myelo-, and chemoarchitecture, were found to be very similar to that observed in commonly studied mammals. Minor variations, such as less nuclear parcellation in the bed nuclei of the stria terminalis, may represent species-specific variations, or may be the result of the limited range of stains used. Given the overall similarity across mammalian species, it appears that the subpallial telencephalon of the mammalian brain is highly conserved in terms of evolutionary changes detectable with the methods used. It is also likely that the functions associated with these nuclei in other mammals can be translated directly to

Abbreviation: 3V, third ventricle; ac, anterior commissure; Acb, accumbens nucleus; AcbC, accumbens nucleus, core; AcbSh, accumbens nucleus, shell; Amyg, amygdaloid body; BAC, bed nucleus of the anterior commissure; BNST, bed nuclei of the stria terminalis; C, caudate nucleus; CB, cell bridges of the ventral striatum; cc, corpus callosum; ChAT, choline acetyltransferase; cst, commissural stria terminalis; df, dorsal fornix; DP, dorsal peduncular cortex; DT, dorsal thalamus; En, endopiriform nucleus; EGP, external globus pallidus; ESl, external septal lamina; f, fornix; fi, fimbria of the hippocampus; HDB, nucleus of the horizontal limb of the diagonal band of Broca; Hip, hippocampal formation; Hyp, hypothalamus; ic, internal capsule; ICj, islands of Calleja; ICjM, islands of Calleja, major island; IG, indusium griseum; IGP, internal globus pallidus (intrapeduncular nucleus, entopeduncular nucleus); Ld, lambdoid septal zone; lot, lateral olfactory tract; LPO, lateral preoptic area; LSD, lateral septal nucleus, dorsal part; LSI (1-4)lateral septal nucleus, intermediate part, layers 1, lateral septal nucleus, intermediate part, layers 14.; LSS, lateral stripe of the striatum; LSV, lateral septal nucleus, ventral part; LTer, lamina terminalis; LV, lateral ventricle; NeuN, neuronal nuclear marker; MnPO, median preoptic nucleus; MPO, medial preoptic area; MS, medial septal nucleus; N.Bas, nucleus basalis; NLOT, nucleus of the lateral olfactory tract; Nv, navicular nucleus of basal forebrain; OC, optic chiasm; P, putamen nucleus; PIR, piriform cortex; PLd, paralambdoid septal nucleus; Pr, principal (encapsulated) nucleus of the bed nucleus of the stria terminalis; PtRl, para-tractal region of the bed nucleus of the stria terminalis, lateral division; PtRm, para-tractal region of the bed nucleus of the stria terminalis, medial division; R, thalamic reticular nucleus; RI, bed nucleus of the stria terminalis, rostral intermediate division; RL, bed nucleus of the stria terminalis, rostral lateral division; RM, bed nucleus of the stria terminalis, rostral medial division; RtSt, reticulostrial nucleus; S, septal nuclear complex; SEd, striatal extension of the bed nucleus of the stria terminalis, dorsal division; SEdc, striatal extension of the bed nucleus of the stria terminalis, dorsal division, core subdivision; SEds, striatal extension of the bed nucleus of the stria terminalis, dorsal division, surround subdivision; SEv, striatal extension of the bed nucleus of the stria terminalis, ventral division; SEvc, striatal extension of the bed nucleus of the stria terminalis, ventral division, core subdivision; SEvs, striatal extension of the bed nucleus of the stria terminalis, ventral division, surround subdivision; SFi, septofimbrial nucleus; SFO, subfornical organ; SHi, septohippocampal nucleus; SHy, septohypothalamic nucleus; SIB, substantia innominata, basal part; sm, stria medullaris of the thalamus; SMc, nucleus of the stria medullaris, compact division; SMd, nucleus of the stria medullaris, diffuse division; st, stria terminalis; Tu, olfactory tubercle; Tu1, olfactory tubercle, layer 1; Tu2, olfactory tubercle, layer 2; Tu2, olfactory tubercle, layer 2; TS, triangular septal nucleus; VDB, nucleus of the vertical limb of the diagonal band of Broca; vGlut2, vesicular glutamate transporter 2; VP, ventral pallidum; ZL, zona limitans.

the tree pangolin, albeit with the understanding that the stimuli that produce activity within these regions may be specific to the life history requirements of the tree pangolin.

KEYWORDS
bed nuclei of the stria terminalis, carnivora, cholinergic basal forebrain, Pholidota, septal nuclei, striatopallidal complex

1 | INTRODUCTION

The vertebrate telencephalon develops from the prosencephalic, or forebrain, vesicle, which subsequently compartmentalizes into the secondary prosencephalon and diencephalon, with the secondary prosencephalon developing into the telencephalic and hypothalamic fields (Watson et al., 2017). The telencephalic field consists of a caudal region from which the pallium emerges and a rostral region that develops into the subpallium. The developing subpallium is arranged into a series of anteroposterior bands (including the preoptic area, diagonal domain, pallidum, and striatum), two dorsoventral entities (from which the septum and subpallial amygdala develop), as well as the paraseptal entity (involved in the development of the nucleus accumbens [Acb]) (Watson et al., 2017). This developmental process leads to the formation of the septal region (as defined by Risold, 2004) and the striatopallidal complex (as defined by Chen et al., 2020), although the precise definition of what portions of the subpallium are considered to part of which nuclear complex and their associated development origins remains somewhat unclear (Watson et al., 2017). This is especially so in terms of the regional assignation of components of the extended amygdala (e.g., de Olmos et al., 2004).

The neurons of the subpallium are involved in a broad range of neural processes essential for survival. The septal nuclear complex is heavily interconnected with the hippocampal formation and the hypothalamus, with the lateral septum being involved in the processing of mood, motivation, and movement (Wirtshafter & Wilson, 2021). The basal forebrain cholinergic nuclei are involved in functions associated with attention (e.g., Villano et al., 2017). The bed nuclei of the stria terminalis (BNST) are involved in limbic functions and valence monitoring (e.g., Lebow & Chen, 2016), and the dorsal and ventral regions of the striatopallidal complex are involved in motor/cognitive and motivation/reward/emotion functions, respectively (e.g., Chen et al., 2020).

While the subpallial telencephalon of the tree pangolin appears to house the full range of structures typically identified in mammals (e.g., Radtke-Schuller, 2018), and these appear to occupy the relative positions typically observed across mammals (Imam et al., 2017; Imam et al., 2018a), no detailed description of the tree pangolin subpallial telencephalon has been provided to date. Here, we continue our detailed anatomical description of the structure of the brain of the tree pangolin (Imam et al., 2017; Imam et al., 2018a; Imam et al., 2018b; Imam et al., 2019a; Imam et al., 2019b; Imam et al., 2019c; Imam, Bhagwandin, Ajao & Manger, 2022) by providing a comprehensive account of the structures observed in the subpallial telencephalon, including aspects of the extended amygdala that were not included in our description of the amygdaloid body (Imam et al., 2022).

2 | MATERIALS AND METHODS

2.1 | Specimens

Adult tree pangolins (*Manis tricuspis*), caught from wild populations in Esejire, Osun State, Nigeria, were used in the current study (see Imam et al., 2017). Permission to obtain the live pangolins and export the prepared tissue from Nigeria for noncommercial, scientific research was granted by the CITES Management Authority, Federal Department of Forestry, Federal Ministry of Environment, Nigeria (Permit No: NG.07.16). Importation of the formalin fixed tissues into South Africa for scientific research purposes was obtained from the National CITES Management Authority, Department of Environmental Affairs, South Africa (Permit No: 152626), and the Department of Agriculture Forestry and Fisheries, South Africa (Permit No: 13/1/1/30/2/0-201608002976). All animals were treated and used according to the guidelines of the University of the Witwatersrand Animal Ethics Committee (AESC No. 2012/53/01), which parallel those of the NIH for the care and use of animals in scientific experimentation. In the current study, the brains of three of these tree pangolins (MT1, MT3, and MT5; see Imam et al., 2017) were sectioned, stained, and analyzed.

2.2 | Sectioning and immunohistochemical staining

Prior to sectioning, each brain was allowed to equilibrate in 30% sucrose in 0.1 M PB at 4°C. The brains were then frozen in crushed dry ice and sectioned into 50-μm-thick sections on a freezing microtome. The whole brain of MT1 was sectioned in the coronal plane and a 1 in 10 series of sections taken and stained for Nissl, myelin, tyrosine hydroxylase (TH), orexin-A (OxA), serotonin (5HT), parvalbumin (PV), calbindin (CB), calretinin (CR), neurofilament H (NFH), and vesicular glutamate transporter 2 (vGlut2). The whole brain of MT3 was sectioned in the coronal plane and a 1 in 5 series of sections taken and stained for neuronal nuclear marker (NeuN), choline acetyltransferase (ChAT), PV, CB, and CR. The right half of the brain of MT5 was sectioned in the sagittal plane and a 1 in 10 series of sections taken and stained for Nissl, myelin, TH, 5HT, PV, CB, CR, NFH, vGlut2, and doublecortin (DCX). Complete details of staining for Nissl and myelin staining, antibody

TABLE 1 Sources and dilution of antibodies used in the current study

Antibody	Host	Immunogen	Manufacturer	Catalogue No.	Reference	Dilution	RRID
ChAT	Goat	Human placental enzyme	Merck-Millipore	AB144P	Laux et al. (2012); Kaiser et al. (2011)	1:3000	AB_2079751
TH	Rabbit	Purified tyrosine hydroxylase from rat adrenal	Merck-Millipore	AB151	Piskuric et al., 2011	1:3000	AB_10000323
OxA	Rabbit	Synthetic peptide corresponding to the c-terminal portion of bovine orexin-A peptide	Merck-Millipore	AB3704	Li & Kiruoac, 2008	1:3000	AB_91545
5HT	Rabbit	Serotonin covalently bound to bovine thyroglobulin with carbodiimide	Merck-Millipore	AB938	Not available	1:5000	Not available
PV	Rabbit	Rat muscle parvalbumin	Swant	PV28	Hirano et al., 2011	1:10,000	AB_10000343
CB	Rabbit	Rat recombinant calbindin D-28k	Swant	CB38a	Bunce et al., 2013	1:10,000	AB_10000340
CR	Rabbit	Recombinant human calretinin containing a 6-his tag at the N-terminal	Swant	7699/3H	Adrio et al., 2011	1:10,000	AB_10000321
vGlut2	Mouse	Recombinant protein from rat vGlut2	Merck-Millipore	MAB5504	Wong et al., 2008; Griffin et al., 2010	1:4000	AB_2187552
SMI-32	Mouse	Non-phosphorylated epitope of neurofilament H from rat hypothalami	Covance	SMI-32R	Sternberger & Sternberger, 1983	1:1000	AB_509997
NeuN	Rabbit	GST-tagged recombinant protein corresponding to mouse NeuN	Merck-Millipore	ABN78C3	Ngwenya et al., 2016	1:500	AB_11204707
DCX	Goat	c-Terminus of doublecortin of human origin	Santa Cruz Biotechnology	sc-8006	Brown et al., 2003; Patzke et al., 2015	1:300	AB_2088494

characterization, specificity, and the protocol followed for all immunostains listed above, have been provided previously (Imam et al., 2018a; Table 1).

2.3 | Analysis and iconography

A low-power stereomicroscope was used to examine the sections and camera lucida drawings of the sections, outlining architectural borders, were made. Architectonic borders of the septal nuclei, basal forebrain, and BNST were first defined using the standard Nissl and myelin stains (Figure 2). The parcellation of the nuclear and cortical regions of the septal nuclei and cortical regions was then confirmed and refined using the immunohistochemical stains. In addition, where relevant, cholinergic neurons were marked on these drawings. The drawings were then scanned and redrawn using the Canvas Draw 6 program (Canvas GFX, Inc., FL, USA). The nomenclature used in the current study was based primarily on that used by Paxinos et al. (2009). While the terminology applied to the regions analyzed herein is variable across studies and species, where the terminology used in these studies was not appropriate to the current findings, we used the most appropriate terminology available (e.g., Ju & Swanson, 1989). Digital photomicrographs were captured using a Zeiss Axioskop. No pixilation adjustments or manipulation of the captured images were undertaken, except for the adjustment of contrast, brightness, and levels using Adobe Photoshop.

3 | RESULTS

As briefly described previously (Imam et al., 2017, 2018a), the subpallial telencephalon of the tree pangolin does not appear to show any major variations in terms of the nuclear complexes present and the topographical arrangement of these complexes. In addition, within the nuclear complexes, the constituent nuclei and their internal topographical relationships appear similar to what has described in other mammals (e.g., Paxinos et al., 2009; Radtke-Schuller, 2018). Here, we provide comprehensive descriptions of the septal region (as defined by Risold, 2004) and the structures forming the ventral and dorsal regions of the striatopallidal complex (as defined by Chen et al., 2020).

3.1 | The septal region

Risold (2004) has defined the septal region of the mammalian brain as being composed of four groups: medial, lateral, posterior, and ventral.

In the tree pangolin, the septal region occupied the medial wall of the cerebral hemisphere. Within the septal region of the tree pangolin, we could identify all the nuclei that form the four groups as defined by Risold (2004).

3.1.1 | The medial septal group

The medial septal group comprises of the medial septal nucleus (MS) and the nucleus of the diagonal band (of Broca) (Risold, 2004). The MS was observed within the anteromedial portion of the septal nuclear complex (Figures 1(d)–1(j)). The MS was populated by a moderate density of neurons, ranging in relative size from larger to smaller (Figure 2(a)). Throughout the MS, a high density of myelinated fibers was observed (Figure 2(b)) and this nucleus contained a moderate density of cholinergic neurons (Figure 2(c)). A low density of relatively larger PV-immunopositive neurons, as well as a moderate to high density of PV-immunopositive terminal networks and other structures were observed (Figure 2(d)). A low density of relatively smaller neurons immunopositive for CB (Figure 2(e)) and CR were present, as well as a moderately dense CR-immunopositive terminal network (Figure 2(f)). A moderate density of relatively larger neurons and other structures immunopositive for NFH were observed (Figure 2(g)), as well as a moderate density of axon terminals immunopositive for vGlut2 (Figure 2(h)). This combination of cyto-, myelo-, and chemoarchitectural features allowed the accurate identification of the location and extent of the MS.

The nucleus of the diagonal band (of Broca) in the brain of the tree pangolin was located in the ventromedial aspect of the telencephalic hemisphere topographically anterior to the hypothalamus (Figures 3(i)–3(l) and 4), as is typically observed in mammals (e.g., Paxinos et al., 2009). In the tree pangolin, both the nucleus of the vertical limb of the diagonal band of Broca (VDB) and nucleus of the horizontal limb of the diagonal band of Broca (HDB) could be identified (Figure 4). In both the VDB and HDB, a substantive density of multipolar neurons of various relative sizes, with dendritic branches primarily oriented parallel to the curved surface of the ventromedial telencephalon, was observed (Figures 4(a), 4(e), and 4(f)). A sizeable subset of these neurons, mostly those of larger relative size, were cholinergic in both nuclei (Figures 4(b), 4(g), and 4(h)). No significant populations of PV- or CR-immunopositive cells were noted in either nucleus, although scattered cells and abundant neuropil were immunopositive for NFH in both nuclei (Figures 4(d), 4(k), and 4(l)). Throughout both the VDB and HDB, a subset of relatively smaller neurons were CB-immunopositive (Figures 4(c), 4(i), and 4(j)), and in the HDB, several relatively larger neurons were CB immunopositive, but these relatively larger CB-immunopositive neurons were not observed in the VDB (Figures 4(c), 4(i), and 4(j)). This combination of features allowed the ready delineation of the nucleus of the diagonal band and the parcellation of this nucleus into distinct vertical and horizontal limbs.

3.1.2 | The lateral septal group

The lateral septal group comprises of the lateral septal nucleus, the septofimbrial nucleus (SFi), and the septohippocampal nucleus (SHi) (Risold, 2004), all of which were identified in the tree pangolin; however, it must be noted that the SFi and SHi appear to be part of the pallial septum (Abellán et al., 2010; Abellán et al., 2014) rather than part of the subpallial septum as designated herein. While not specifically defined as belonging to the lateral septal group (Medina & Abellán, 2012), based on their topographical location we include the septohypothalamic nucleus (SHy), the lambdoid septal zone (Ld), and the paralambdoid septal nucleus (PLd) as components of this group for the purposes of the current description. The lateral septal nucleus was observed to be composed of seven distinct parts, a dorsal part (LSD), a ventral part (LSV), an intermediate part composed of four layers (LSI1—4), and the external septal lamina (ESl) (Figures 1(d)–1(m)). The LSD occupied the dorsal lateral aspect of the septal region throughout its rostrocaudal extent (Figures 1(d)–1(m)). Similarly, the LSV occupied the ventral lateral aspect of the septal region throughout the majority of its rostrocaudal extent (Figures 1(d)–1(k)). Both nuclei were bordered medially by the LSI and laterally by the ESI (Figure 1). The neuronal complements of both the LSD and LSV appeared quite similar, and displayed a range of neuronal sizes, shapes, and types (Figures 5(a) and 5(e)). In contrast, the LSD exhibited a substantially denser myelin staining that the LSV (Figures 5(b) and 5(f)), a lower intensity of CB-immunopositive neuropil staining (Figures 5(c) and 5(g)), and a lower density of CR-immunopositive neurons (Figures 5(d) and 55(h)) than the LSV.

The LSI occupied the majority of the lateral septal nucleus (Figures 1(d)–1(m)) and four layers (layers 1—4, layer 1 being the most lateral, 4 the most medial) were observed (Figure 6). Through the LSI a moderate density of neurons ranging in relative size were observed (Figure 6(a)). There was a tendency for the neurons in layers 1 and 2 to be relatively larger than those observed in layers 3 and 4 (Figure 6(a)). The density of myelin was lowest in layer 1, gradually reaching a quite high density in layer 4 (Figure 6(b)). The density of PV-immunopositive structures was low in layers 1, 2 and 4, but within layer 3, a high-density PV-immunopositive terminal network is seen to clearly demarcate this layer (Figure 6(c)). Low densities of relatively small CB-immunopositive neurons were observed in layers 1, 2, and 4, but these were not observed in layer 3 (Figure 6(d)). A low density of relatively larger CR-immunopositive neurons was observed in layers 1 and 2, with no neurons observed in layer 3, while in layer 4, a low density of relatively smaller CR-immunopositive neurons was seen (Figure 6(e)). A low density of NFH-immunopositive structures was observed in layers 1–3, with a slight increase in density of these structures in layer 4 (Figure 6(f)). Throughout the four layers, a moderate density of vGlut2-immunopositive boutons was noted, and in layer 1, a very low density of neurons exhibited vGlut2-immunopositive pericellular baskets that was not observed in the other layers (Figure 6(g)). This range of features allowed the accurate demarcation of the lateral septal nucleus and its constituent layers.

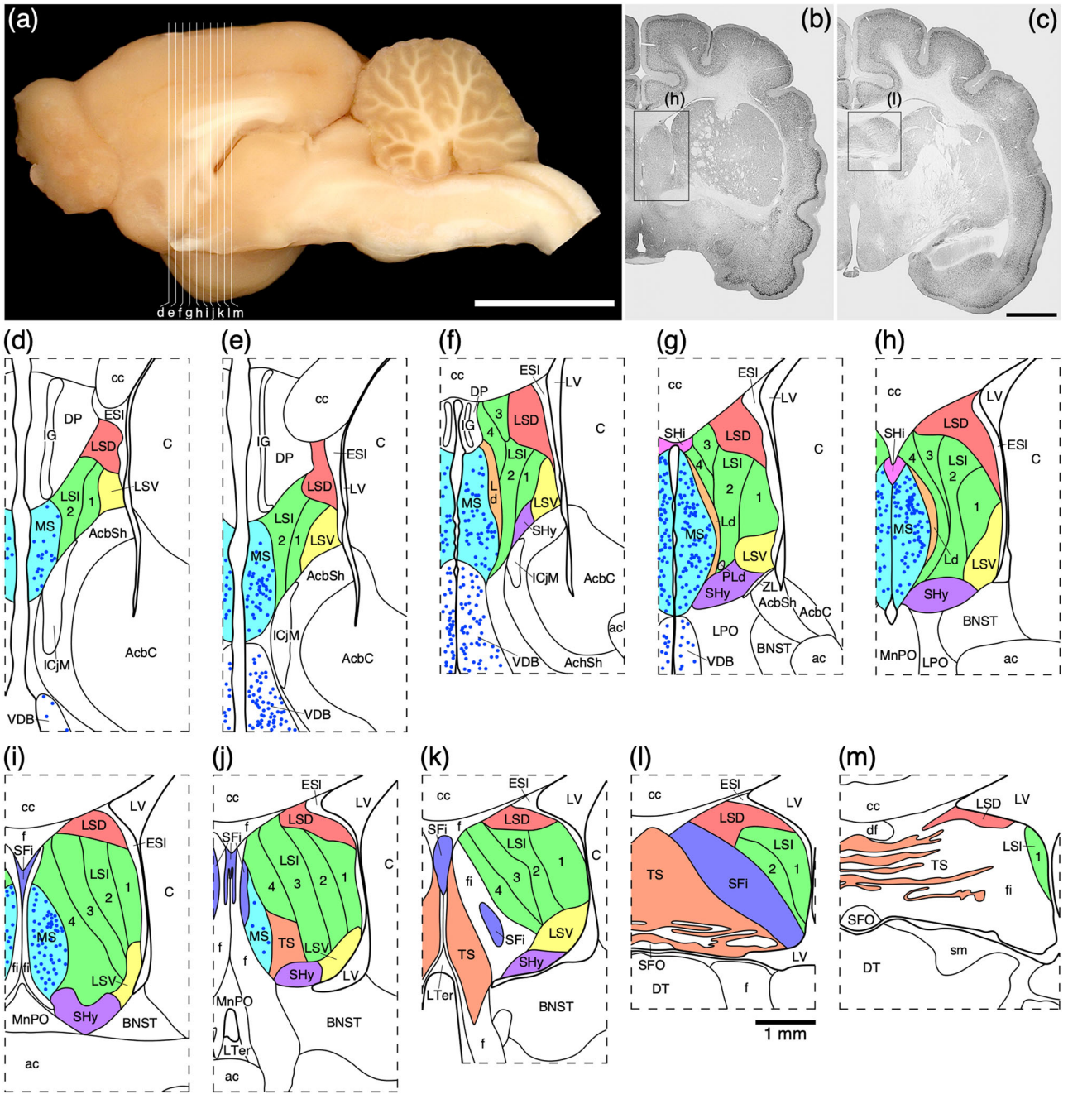

FIGURE 1 (a) Photograph of the mid-sagittal plane of the brain of the tree pangolin showing the level at which the coronal sections imaged (b and c) and reconstructed (d–m) were taken. Scale bar in (a) = 1 cm and applies to (a) only. (b and c) Photomicrographs of coronal sections through the tree pangolin telencephalon, taken at the levels corresponding to (h) and (l) in (a), showing examples of the regions that were magnified and reconstructed (boxed regions), in these two cases figurines (h) and (l) specifically. Scale bar in (c) = 3 mm and applies to (b) and (c). (d–m) Diagrammatic reconstructions showing the nuclear organization of the septal nuclear complex of the tree pangolin. In all figurines, dorsal is to the top and medial to the left. Figurine (d) represents the most rostral portion of the septal nuclear complex, whereas figurine (m) represents the most caudal portion. Each figurine is approximately 500 μm apart. The various nuclei/nuclear groups of the septal nuclear complex are represented with differing colors. Choline acetyltransferase immunopositive neurons in the medial septal nucleus (MS) and the vertical diagonal band (VDB) are represented with blue dots, each dot representing a single neuron. See list for abbreviations

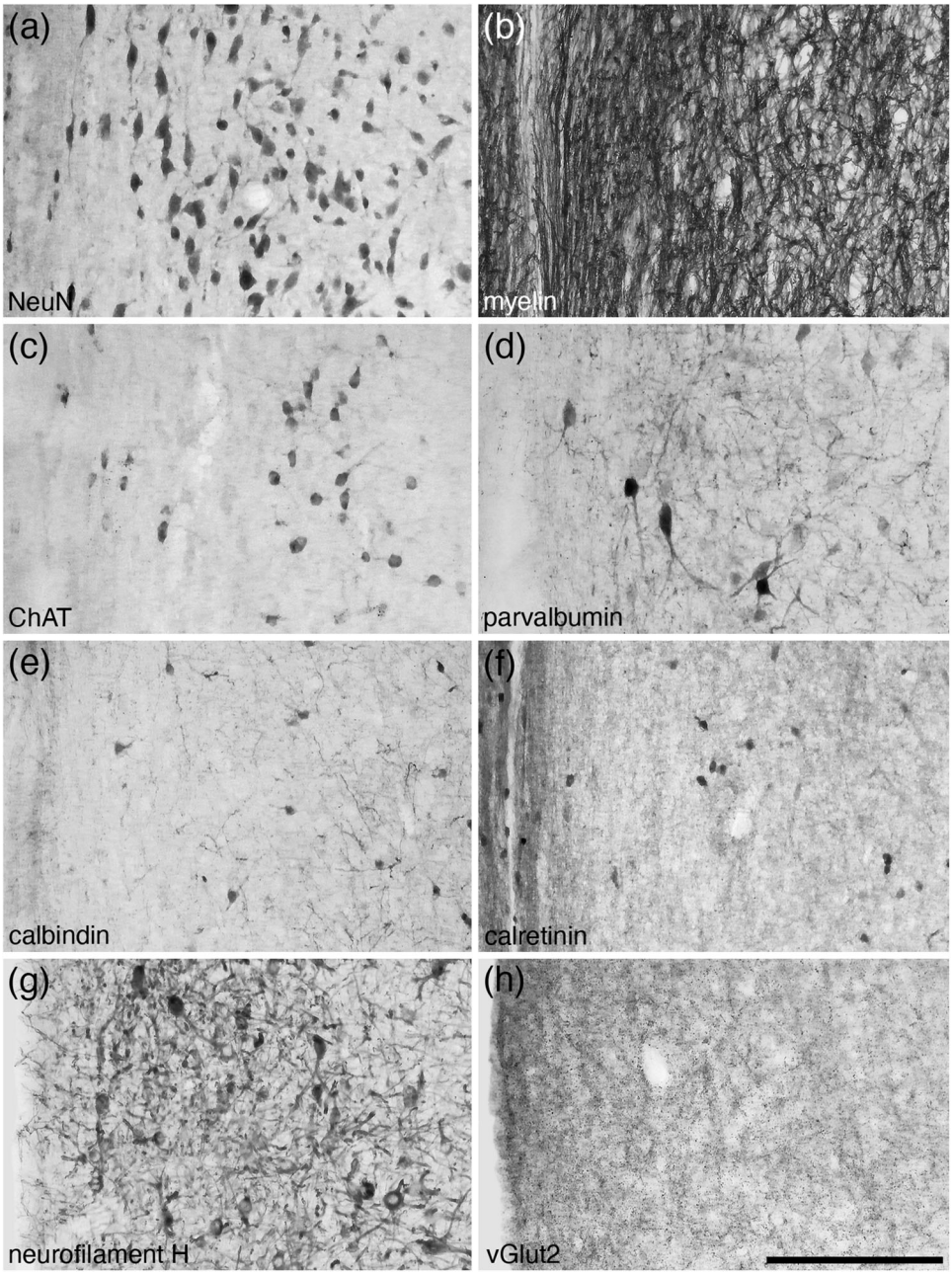

FIGURE 2 Photomicrographs of coronal sections through the medial septal nucleus of the tree pangolin stained for neuronal nuclear marker (NeuN, a), myelin (b), choline acetyltransferase (ChAT, c), parvalbumin (d), calbindin (e), calretinin (f), neurofilament H (g), and vesicular glutamate transporter 2 (vGlut2, h). The combination of distinct features depicted in this plate, such as a high myelin density (b), the presence of cholinergic neurons (c), and substantive densities of parvalbumin (d) and neurofilament H (g) immunopositive structures, allowed for the accurate identification of the extent of this nucleus. In all images, medial is to the left and dorsal to the top. Scale bar in (h) = 200 μm and applies to all

The lateral, or ventricular, border of the septal nuclear complex was lined by a neuron sparse lamina that we term the ESl (Figures 1(d)–1(l)). This neuron sparse lamina exhibited a low density of myelinated axons (indicating that it is not a white matter tract), lacked PV- and NFH-immunostaining, had a moderately dense CB-immunopositive terminal network, and a low-density CR- and vGlut2-immunopositive terminal network (Figure 6). The ESl appears to be a neuron sparse region of neuropil, and is likely to be composed in part by the ependymal layer of the lateral ventricle.

The SFi was located toward the caudal pole of the septal nuclear complex (Figures 1(c) and 1(i)–1(m)) and was composed of a low density of neurons that appear to be lateral, striated, extensions of the triangular septal nucleus (TS, see below) neurons investing into the fibers forming the fimbria (Figure 7). The dendrites of the SFi neurons

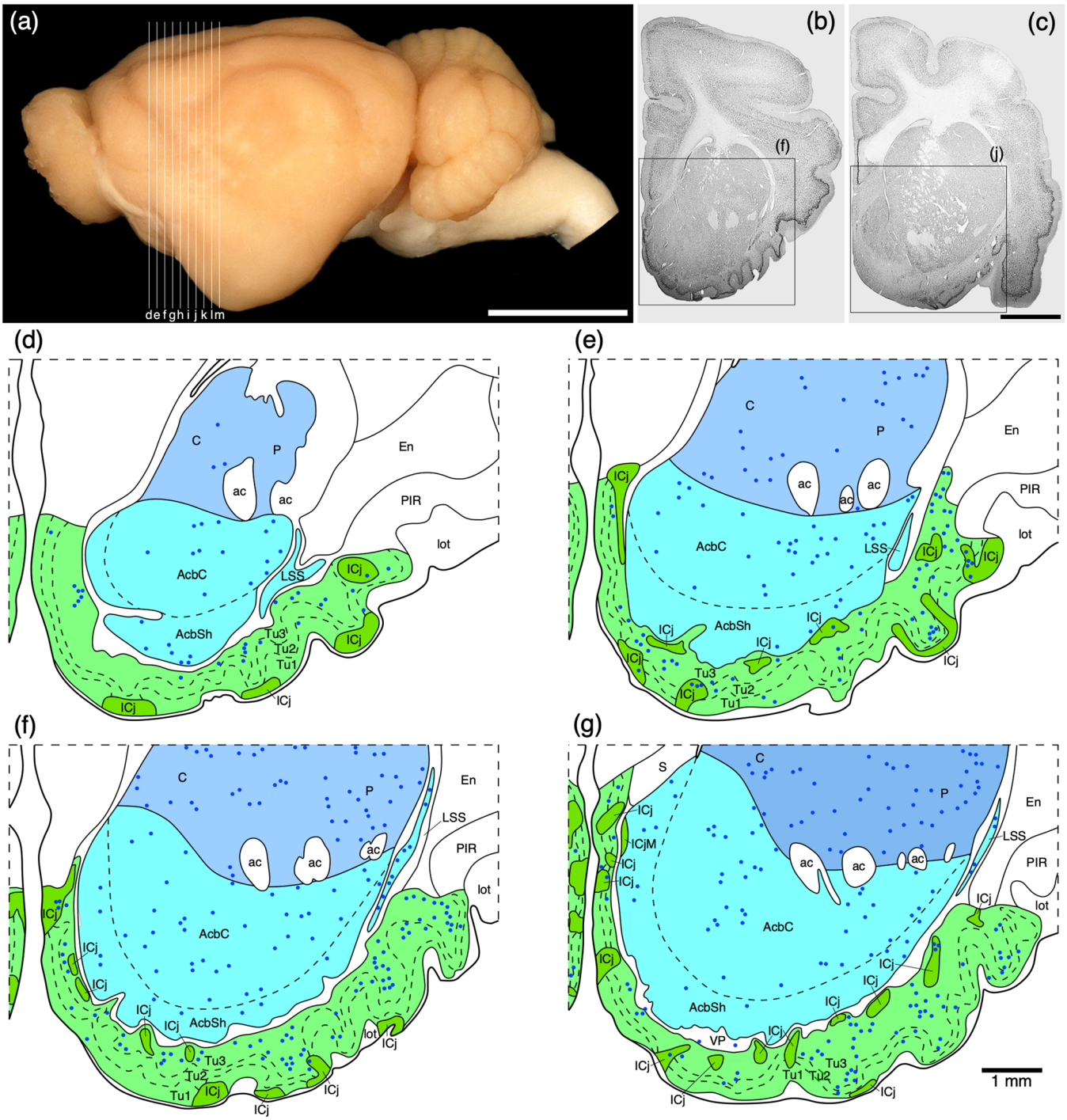

FIGURE 3 (a) Photograph of the lateral aspect of the brain of the tree pangolin showing the levels at which the coronal sections imaged (b and c) and reconstructed (d–m) were taken. Scale bar in (a) = 1 cm and applies to (a) only. (b and c) Photomicrographs of coronal sections through the tree pangolin telencephalon, taken at the levels corresponding to (f) and (j) in (a), showing examples of the regions that were magnified and reconstructed (boxed regions), in these two cases figurines (f) and (j) specifically. Scale bar in (c) = 3 mm and applies to (b) and (c). (d–m) Diagrammatic reconstructions showing the nuclear organization of the cholinergic basal forebrain and ventral striatopallidal complex of the tree pangolin. In all figurines, dorsal is to the top and medial to the left. Figurine (d) represents the most rostral section in which these structures were observed, while figurine (m) represents the most caudal section. Each figurine is approximately 500 μm apart. The various nuclei/nuclear groups are represented with differing colors. Choline acetyltransferase immunopositive neurons are represented with blue dots, each dot representing a single neuron. See list for abbreviations

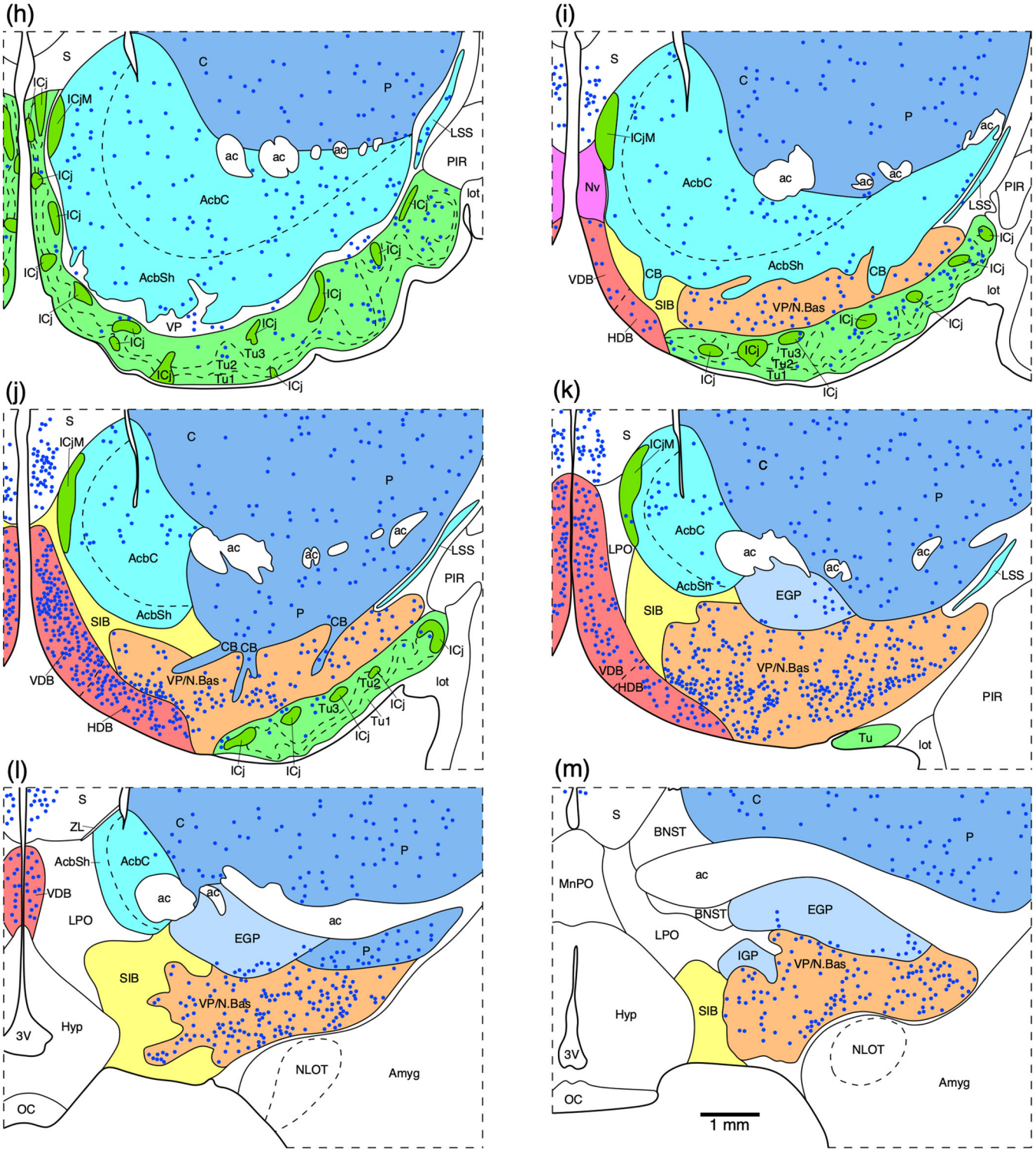

FIGURE 3 Continued

are NFH immunopositive (Figure 7(f)). The neurons within the SFi that are CR immunopositive appear to be slightly larger with more dendritic branches than those of the TS (Figures 7(b) and 7(d)). In addition, a low density of SFi neurons is CB immunopositive, with the entire SFi exhibiting a dense CB-immunopositive neuropil staining (Figure 7(e)).

The SHi was observed to be a very small nucleus located at the dorsomedial border of the complex, located between the MS and the corpus callosum (Figures 1(g) and 1(h)). This small nucleus was formed by a moderate density of neurons, some of which were larger than observed in adjacent nuclei. A high density of myelin was observed in the SHi, as well as a moderate density of NFH- and

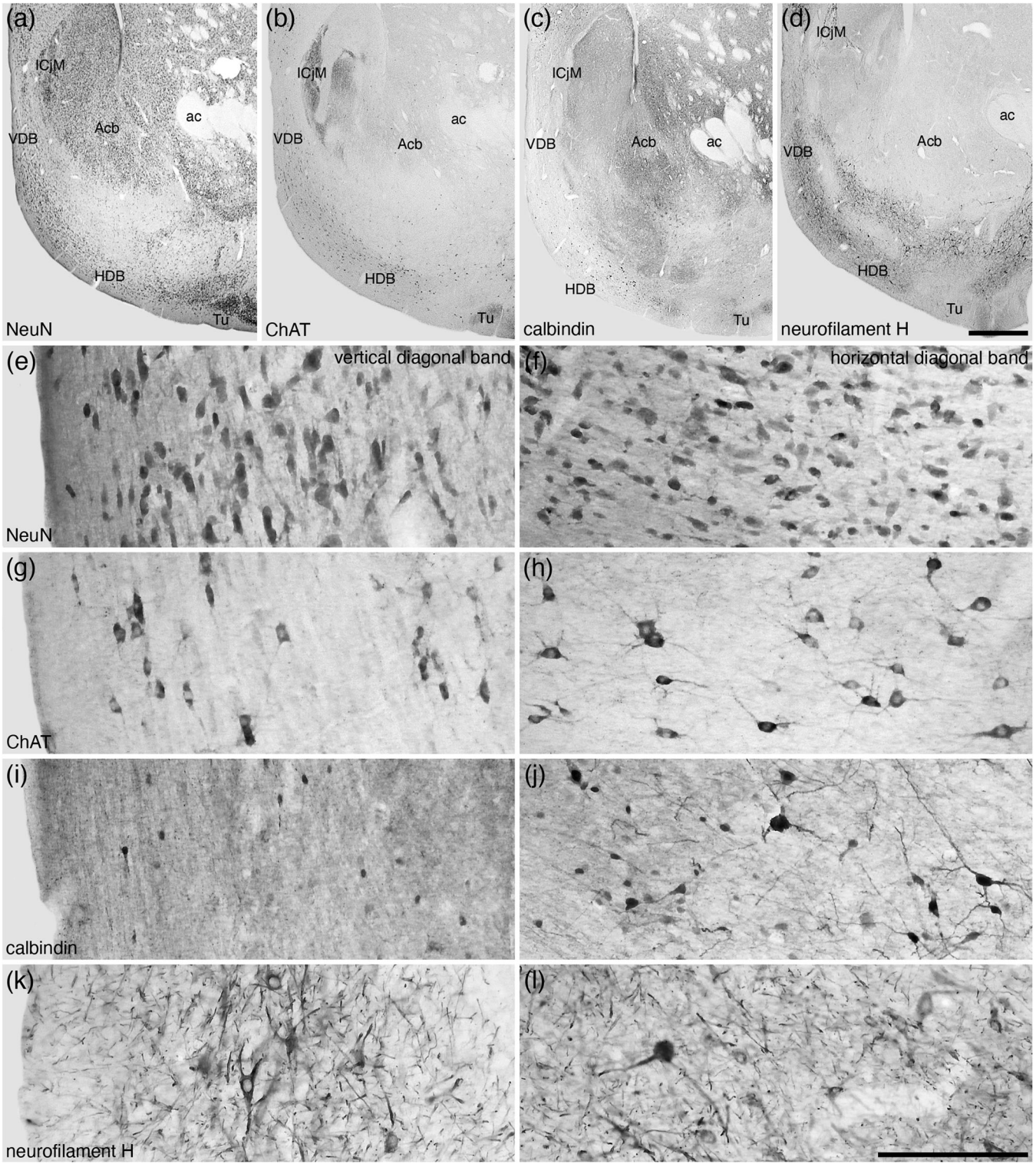

FIGURE 4 Lower (a–d) and higher (e–l) magnification photomicrographs of the nucleus of the diagonal band (of Broca) in coronal sections of the tree pangolin brain stained for neuronal nuclear marker (NeuN; a, e, and f), choline acetyltransferase (ChAT; b, g, and h), calbindin (c, i, and j), and neurofilament H (d, k, and l). Note the presence of numerous cholinergic neurons in both the vertical diagonal band (VDB, Ch2; g) and horizontal diagonal band (HDB, Ch3; h), larger and smaller calbindin immunopositive neurons in the HDB (j) compared with only smaller neurons in the VDB (i), and the numerous structures immunopositive for neurofilament H in both the VDB and HDB (k and l). In all images, medial is to the left and dorsal to the top. Scale bar in (d) = 1 mm and applies to (a)–(d). Scale bar in (l) = 200 μm and applies to (e)–(l). See list for abbreviations

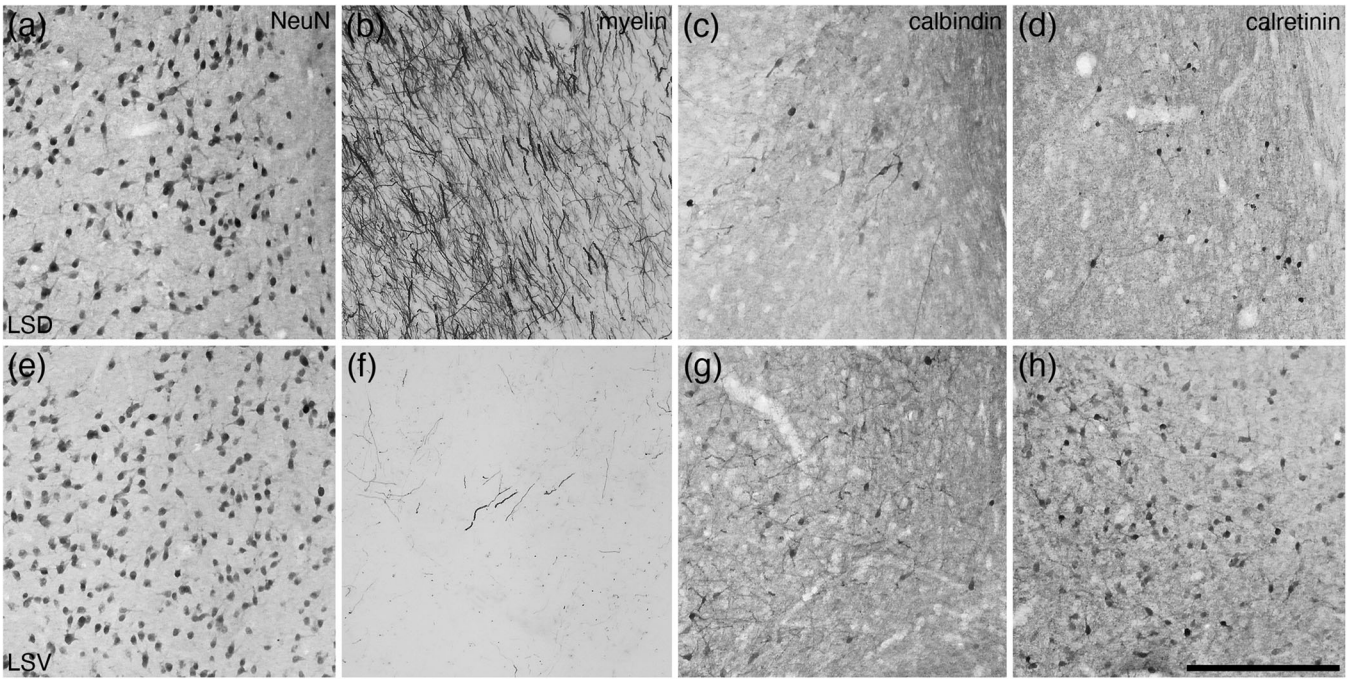

FIGURE 5 Photomicrographs of coronal sections through the lateral septal nucleus, dorsal part (LSD) (a–d) and the lateral septal nucleus, ventral part (LSV) (e–h), stained for neuronal nuclear marker (NeuN; a and e), myelin (b and f), calbindin (c and g), and calretinin (d and h). Clear variations in staining densities for myelin (b and f), calbindin (c and g), and calretinin (d and h) support the division of these regions of the lateral septal nucleus into the two nuclei. In all images, medial is to the left and dorsal to the top. Scale bar in (h) = 250 μm and applies to all. See list for abbreviations

vGlut2-immunopositive structures. A moderately dense PV-immunopositive terminal network, and a few small CB- and CR-immunopositive neurons were also observed in the SHi.

The SHy was located in the ventral aspect of the lateral septal group (Figures 1(f)–1(k)), medial to the LSV, and dorsal the Acb. A moderate density of multipolar neurons was seen within the SHy, with a moderate density of myelin. While no PV-immunopositive neurons were found in the SHy, a few CB- and CR-immunopositive neurons were observed.

The Ld was observed to be a thin, dorsoventrally oriented band bordered medially by the MS and laterally by layer 4 of the LSI (Figures 1(f)–1(h)). Within the Ld, there was a lower neuronal density than observed in adjacent structures, with a lower myelin density than in the MS, but higher myelin density than the LSI4. A very low-density PV-immunopositive terminal network, the occasional CB-immunopositive neuron, a lack of CR-immunuopositive neurons, and low-density staining for NFH and vGlut2 were also identified in the Ld, distinguishing this nucleus from the surrounding structures. The PLd was formed by a small, high-density cluster of neurons located at the ventrolateral edge of the Ld (Figure 1(g)). A moderate density of myelin and vGlut2-immunpositive terminals was observed in the PLd, but no neurons immunopositive for PV, CB, or CR were noted.

3.1.3 | The posterior septal group

The posterior septal group comprises of the TS, the bed nucleus of the stria medullaris, and the bed nucleus of the anterior commissure (BAC) (Risold, 2004), part of which, including the triangular nucleus and bed nucleus of the stria medullaris, appears to be derived from the prethalamic eminence (Alonso et al., 2020). In the tree pangolin, the TS occupied the medial portion of the caudal pole of the septal nuclear complex (Figures 1(c) and 1(i)–1(m)). The TS formed the distinctive eponymous appearance, and was composed of a high density of neurons of similar shape and size (Figures 7(a) and 7(c)), many of which were immunopositive for CR (Figures 7(b) and 7(d)). No distinct immunostaining for PV or CB (Figure 5(e)) was observed in the TS, but a high density of NFH-immunopositive dendrites was observed (Figure 7(f)). The lack of CB immunostaining in the TS was a feature that clearly distinguishes the TS from the SFi (see above) (Figure 7(e)).

The stria medullaris thalami are a prominent white matter tract that passes information from the frontolimbic areas to the habenular nuclear complex (Roddy et al., 2018). The stria medullaris thalami and habenular nuclear complex show a typically mammalian organization in the tree pangolin (Imam et al., 2019b) (Figures 8(k)–8(t)). Within the ventral aspect of the myelinated fibers that form the stria medullaris thalami in the tree pangolin, a substantial number of neurons are observed, and these form the nucleus of the stria medullaris. In the tree pangolin, the nucleus of the stria medullaris appears to be divisible into two distinct parts. Within the ventral aspects of the stria medullaris, the density of neurons is relatively high, and these neurons are relatively closely packed (Figures 9(a), 9(b), and 9(g)). We have termed this portion the compact part of the nucleus of the stria medullaris (SMc). In addition, dorsal to the SMc, scattered neurons are found throughout the myelinated fibers of the stria medullaris,

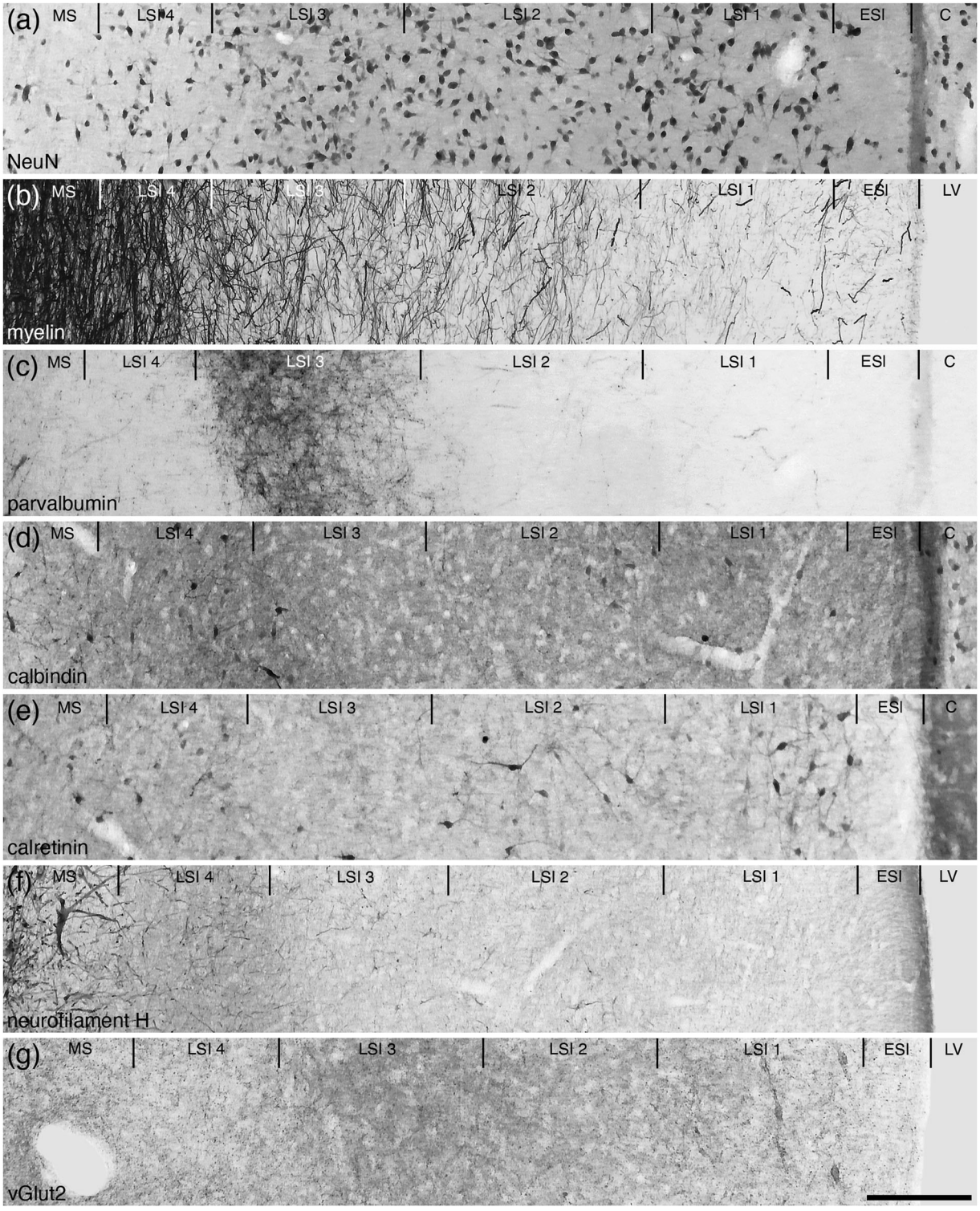

FIGURE 6 Photomicrographs of coronal sections through the lateral septal nucleus, intermediate part (LSI), showing the four distinct layers (LSI 1–4) in the brain of the tree pangolin stained for neuronal nuclear marker (NeuN; a), myelin (b), parvalbumin (c), calbindin (d), calretinin (e), neurofilament H (f), and vesicular glutamate transporter 2 (vGlut2; g). Using this combination of stains, the four layers could be readily discerned. Note the presence of a cell sparse lamina on the lateral, or external, surface of the septal nuclear complex, which we have termed the external septal lamina (ESI). In all images, medial is to the left and dorsal to the top. Scale bar in (g) = 200 μm and applies to all. See list for abbreviations

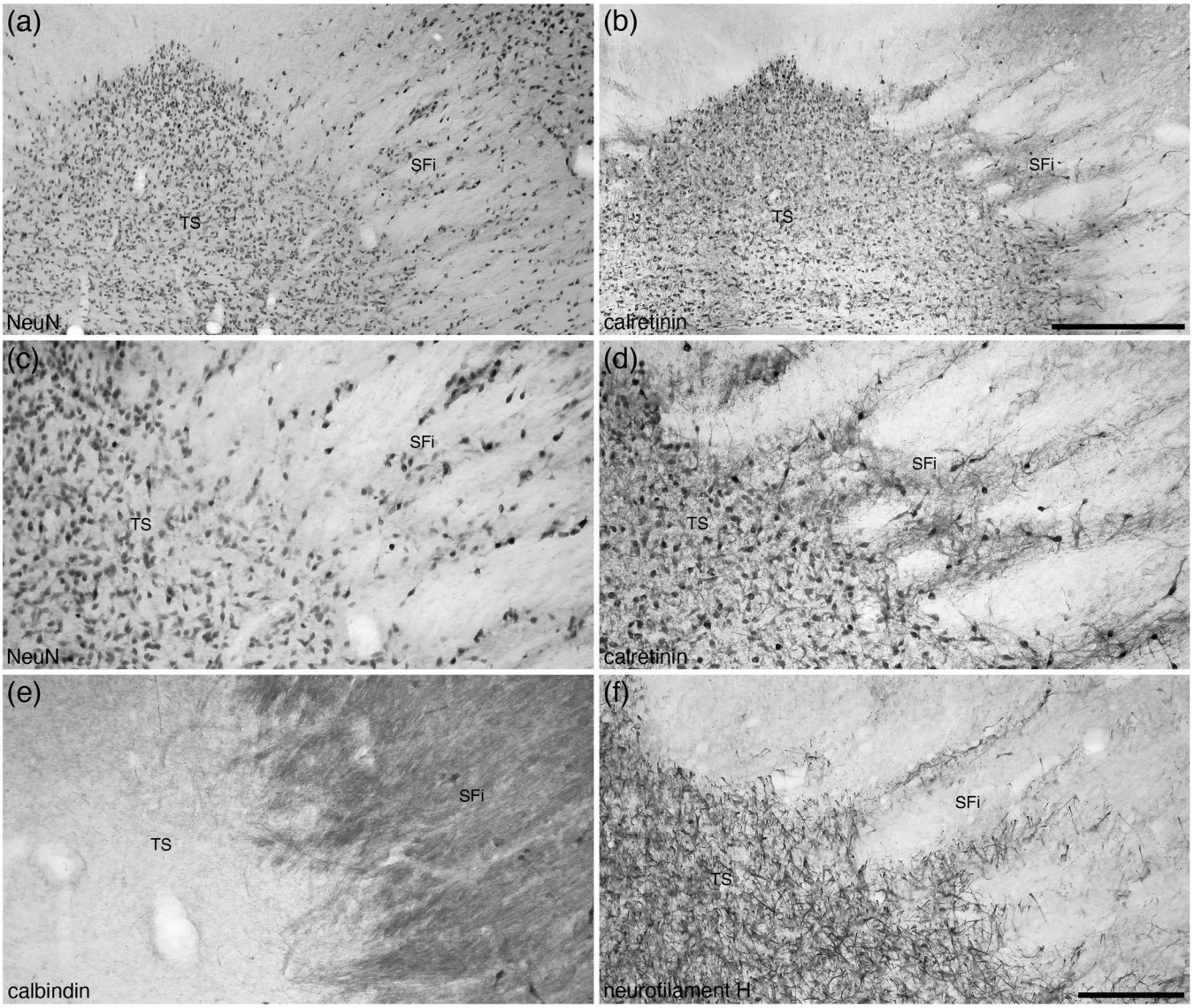

FIGURE 7 Photomicrographs at lower (a and b) and higher (c–f) magnifications of coronal sections through the triangular septal (TS) and septofimbrial (SFi) nuclei of the tree pangolin stained for neuronal nuclear marker (NeuN; a and c), calretinin (c and d), calbindin (e), and neurofilament H (f). Note the distinct triangular shape of the TS, and while the cells forming the striated appearance of the SFi may be interpreted as extensions of the TS neurons (a, c, and f), the difference in morphology of the calretinin neurons (d) between the two nuclei and the difference in calbindin neuropil staining (e) support the distinction of these two nuclei. In all images, medial is to the left and dorsal to the top. Scale bar in (b) = 500 μm and applies to (a) and (b). Scale bar in (f) = 200 μm and applies to (c)–(f)

and these neurons we have termed the diffuse part of the nucleus of the stria medullaris (SMd) (Figures 9(a), 9(b), and 9(g)). Within both the SMc and SMd, the majority of the neurons observed were CR immunopositive (Figures 9(c), 9(f), and 9(h)), and occasional neurons in the more rostral aspects of these nuclear parts are PV immunopositive (Figures 9(b) and 9(e)). No other distinct immunostaining was observed in these nuclei.

The BAC, which lies at the transitional region of the septal nuclei and the preoptic region (Medina & Abellán, 2012), of the tree pangolin was found to lie immediately caudal to the anterior commissure, lateral to the fornix, medial to the BNST, and dorsal to the nucleus of the stria medullaris (Figures 8(i)–8(l)). The BAC was not a large nucleus and exhibited a low density of relatively small neurons (Figure 10(a)), a subset of which were PV immunopositive (Figure 10(b)). The most marked feature of this nucleus was the absence of CB immunostaining (Figure 10(c)), but within this nucleus, several fibers of passage immunopositive for CR were apparent (Figure 10(d)).

3.1.4 | The ventral septal group/BNST

The ventral septal group as defined by Risold (2004) comprises of the BNST, although the BNST are often considered part of the extended amygdala (e.g., Alheid, 2003; de Olmos et al., 2004). In the brain of

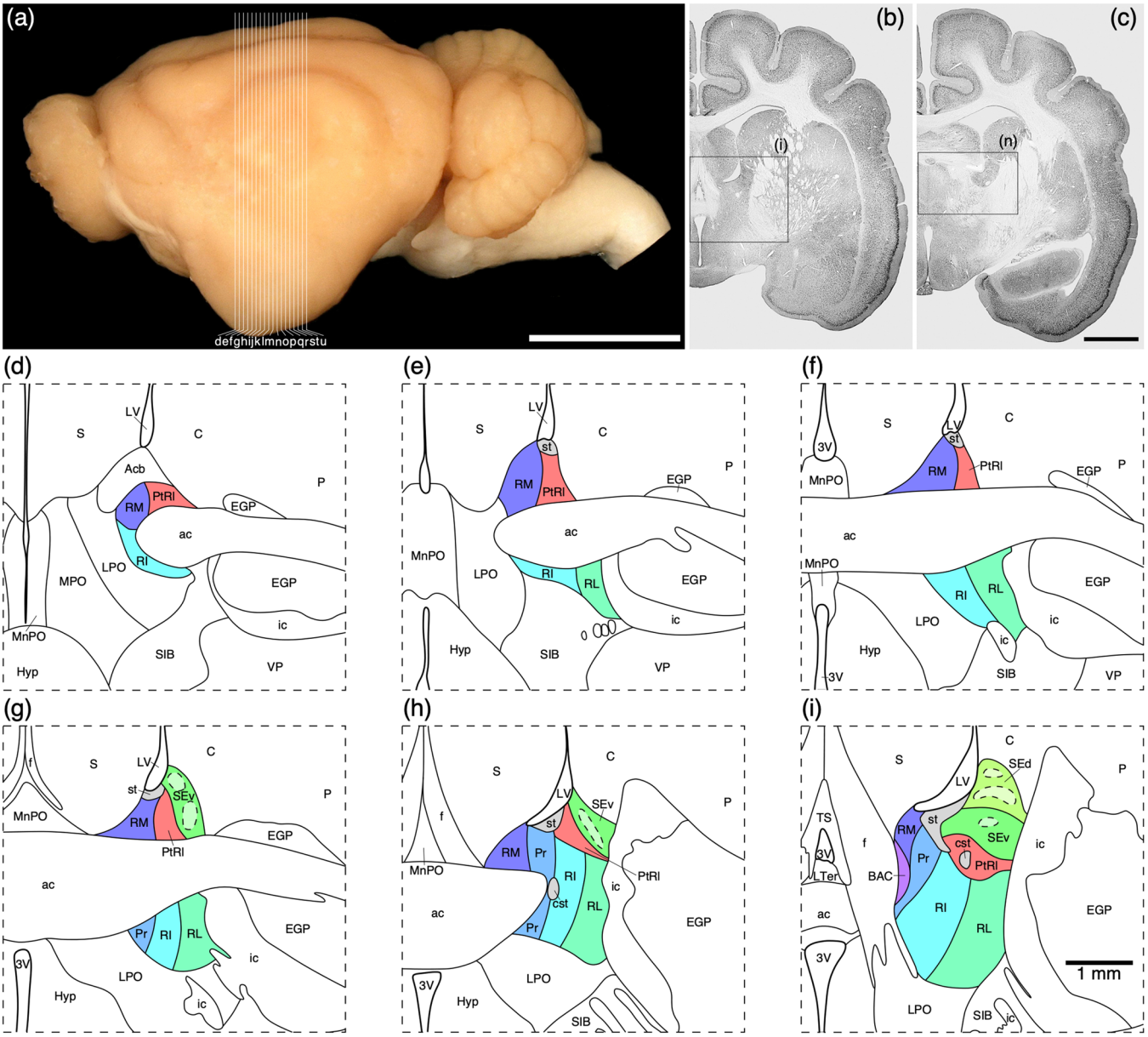

FIGURE 8 (a) Photograph of the lateral surface of the brain of the tree pangolin showing the levels at which the coronal sections imaged (b and c) and reconstructed (d–u) were taken. Scale bar in (a) = 1 cm and applies to (a) only. (b and c) Photomicrographs of coronal sections through the tree pangolin telencephalon, taken at the levels corresponding to (i) and (n) in (a), showing examples of the regions that were magnified and reconstructed (boxed regions), in these two cases figurines (i) and (n) specifically. Scale bar in (c) = 3 mm and applies to (b) and (c). (d–m) Diagrammatic reconstructions showing the organization of the bed nuclei of the stria terminalis (BNST) of the tree pangolin. In all figurines, dorsal is to the top and medial to the left. Figurine (d) represents the most rostral portion of the septal nuclear complex, whereas figurine (u) represents the most caudal portion. Each figurine is approximately 250 μm apart. The various nuclei/nuclear groups of the BNST are represented with differing colors, whereas the associated tracts are in gray. See list for abbreviations

the tree pangolin, the BNST are located immediately caudal to the anterior commissure, positioned between the fornix medially and the internal capsule laterally (Figure 8). Within the BNST, we were able to identify the rostro-ventrally located main cluster of nuclei (comprised of four divisions), the striatal extension (comprised of two subdivisions), and two para-tractal regions. Within the main cluster of nuclei, the four divisions observed, from medial to lateral, include the rostral medial (RM), principal (Pr), rostral intermediate (RI), and rostral lateral (RL) divisions (Figures 8(d)–8(q)). These four divisions form four adjacent, rostroventrally expanded, parallel laminae (Figure 11) that is reminiscent of these nuclei in the rodents (Ju & Swanson, 1989; Paxinos et al., 2009). The RM, located in the dorsomedial aspect of the region (Figure 11), evinces a moderate neuronal density, low myelin density, moderate density of CB-immunopositive neurons, a low to moderate density of CR-immunopositive neurons and axons, a moderate density of OxA-immunopositive axons and boutons, and a very low

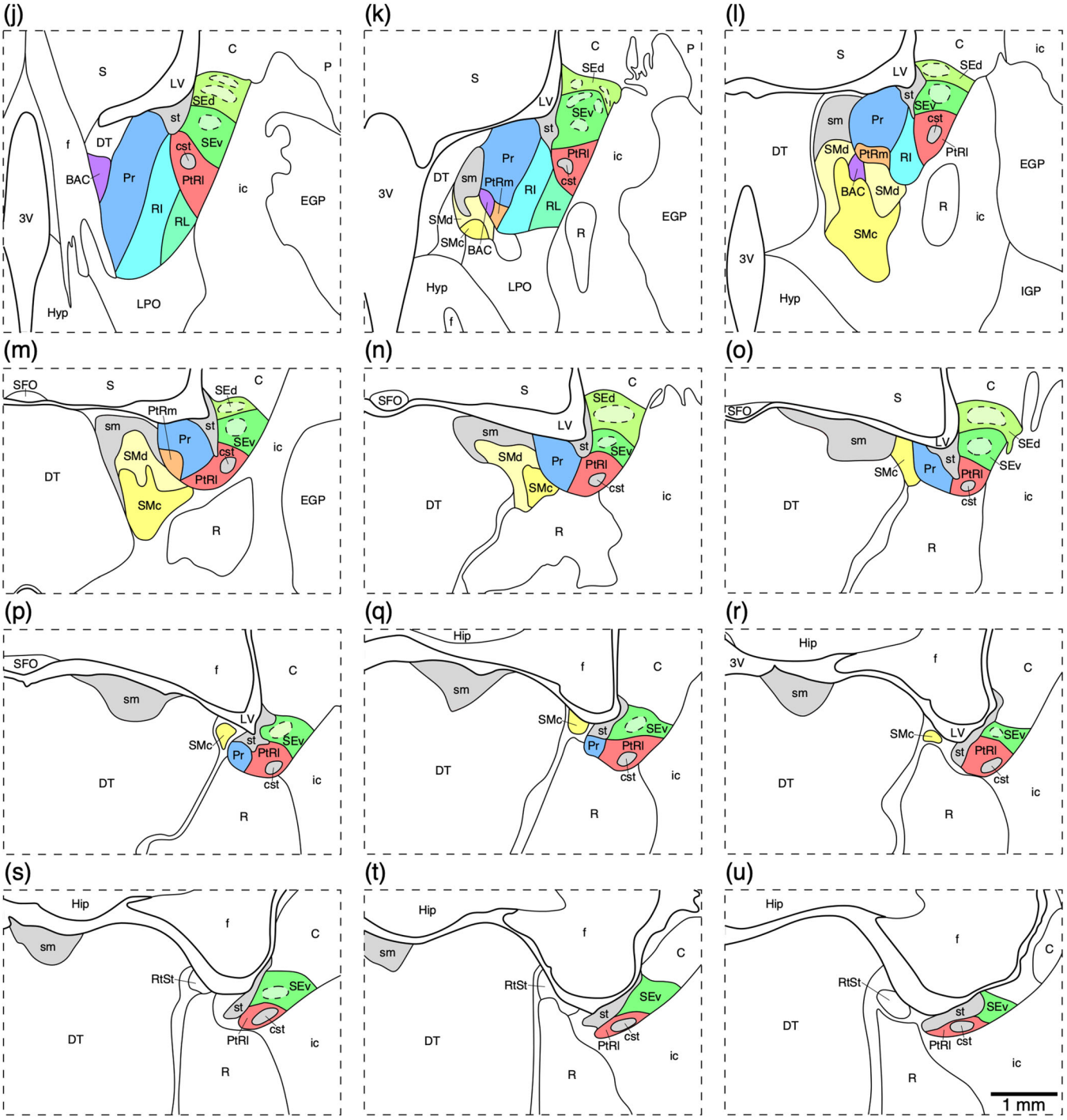

FIGURE 8 Continued

density of NFH-immunopositive dendrites (Figures 11 and 12(a), 12(e), 12(i), 12(m), 12(q), and 12(u)). The Pr exhibited the highest density of neurons, a low myelin density, moderate densities of CB- and CR-immunopositive neurons and axons, a relatively lower intensity of CR-immunostaining of the neuropil, a low density of OxA immunopositive axons and boutons, with occasional neurons and several dendrites immunopositive to NFH (Figures 11 and 12(b), 12(f), 12(j), 12(n), 12(r), and 12(v)). A moderate neuronal and myelin density was observed in the RI, along with a moderate density of CB-immunopositive neurons, a low to moderate density of CR-immunopositive neurons and axons, and a low density of OxA-immunopositive axons and a density of NFH-immunopositive dendrites (Figures 11 and 12(c), 12(g), 12(k), 12(o), 12(s), and 12(w)). The most lateral of these divisions, the RL, evinces a moderate neuronal density and contains occasional larger neurons than observed in the other divisions, a higher myelin density, very few CB-immunopositive neurons, a relatively higher density of

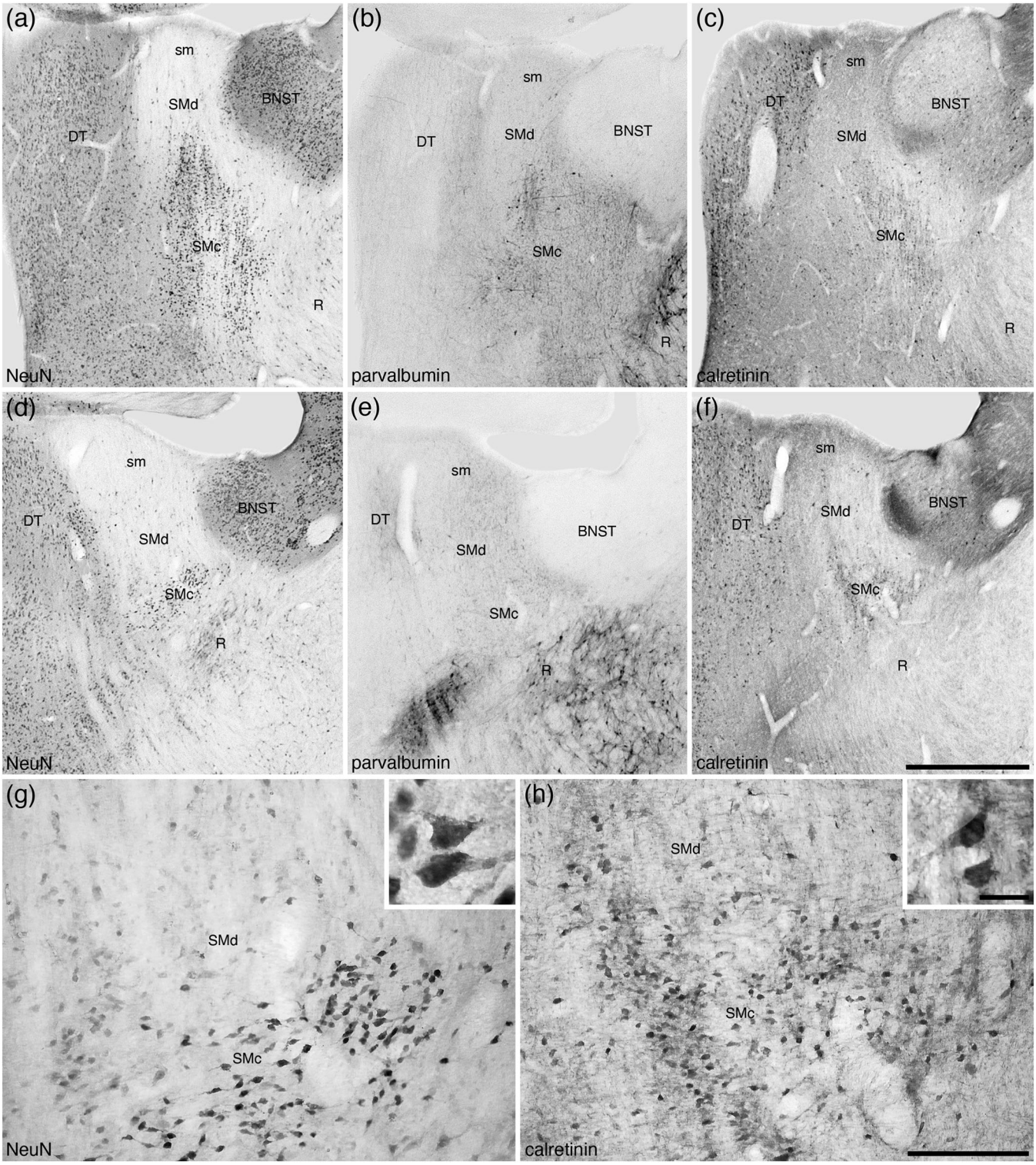

FIGURE 9 Photomicrographs of the nucleus of the stria medullaris (SM) in coronal sections of the tree pangolin brain stained for neuronal nuclear marker (NeuN; a, d, and g), parvalbumin (b and e), and calretinin (c, f, and h). The low magnification images (a–f) represent adjacent sections with different stains (a–c and d–f, with d–f being 250 μm caudal to a–c) to show the location of the SM in relation to the bed nuclei of the stria terminalis (BNST), thalamic reticular nucleus (R), and dorsal thalamus (DT). At higher magnifications, the SM appears divisible into two parts, a compact (SMc) part located ventrally and a diffuse (SMd) part located dorsally and housing far fewer neurons scattered in the fibers of the stria medullaris thalami (sm). The neurons of these two parts of the SM (g) are calretinin immunopositive (h), with scattered neurons in the more rostral parts being parvalbumin immunopositive (b). Insets (g) and (h) are higher magnification images showing the morphology of the neurons in the SMc stained for NeuN (inset g) and calretinin (inset h). In all photomicrographs, medial is to the left of the image and dorsal to the top. Scale bar in (f) = 1 mm and applies to a–f. Scale bar in (h) = 200 μm and applies to (g) and (f). Scale bar in inset (h) = 20 μm and applies to both insets. See list for abbreviations

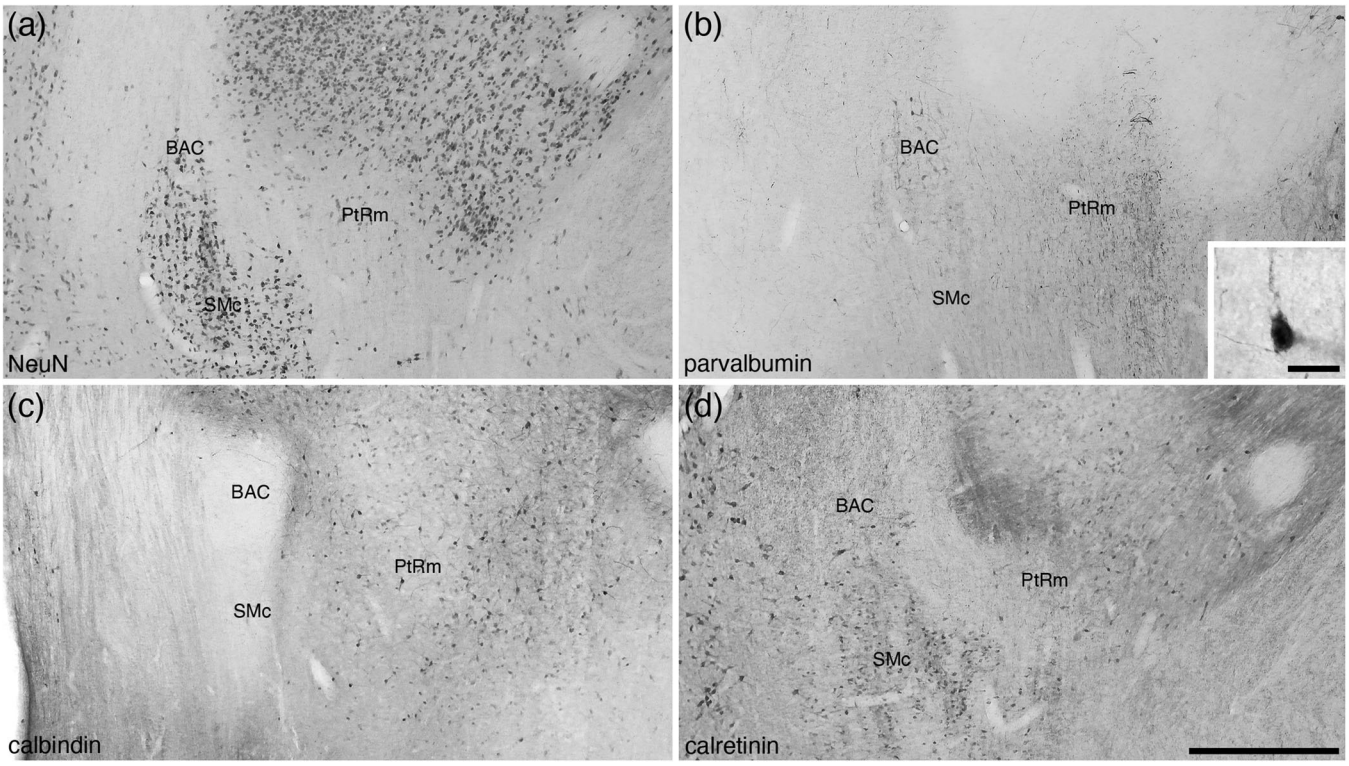

FIGURE 10 Photomicrographs of coronal sections through the bed nucleus of the anterior commissure (BAC) and the medial para-tractal region (PtRm) of the bed nuclei of the stria terminalis of the tree pangolin brain stained for neuronal nuclear marker (NeuN; a), parvalbumin (b), calbindin (c), and calretinin (d). The BAC is not composed of a great number of neurons (a), many of which appear to be parvalbumin-immunopositive (b). PtRm represents a region in the BNST that has a low neuronal density (a, c, and e), but appears to contain many parvalbumin immunopositive fibers (b). In all photomicrographs, medial is to the left and dorsal to the top. Scale bar in (d) = 500 μm and applies to all. Scale bar in inset (b) = 20 μm. See list for abbreviations

CR-immunopositive neurons, a moderate density of OxA-immunopositive axons and boutons, with occasional neurons and several dendrites immunopositive to NFH (Figures 11 and 12(d), 12(h), 12(l), 12(p), 12(t), and 12(x)). The combination of minor variations in the structures revealed with the range of stains used allows for the identification of these four divisions.

At the dorsolateral aspect of the BNST, medioventrally adjacent to the caudate nucleus and internal capsule, we identified the striatal extension of the BNST (Figures 8(g)–8(u)) as defined by Ju and Swanson (1989). Within the striatal extension, we could identify a dorsal (SEd) and ventral (SEv) subdivisions. Within each of these subdivisions, immunostaining revealed distinct core (SEdc and SEvc) and shell (SEds and SEvs) portions. In both the SEd and SEv, a relatively homogeneous density of neurons is observed (Figure 13(a)), although the density appears slightly higher in SEv (Figures 14(a) and 14(c)). In both divisions, the density of myelin is low to moderate, but there appear to be distinct myelinated fascicles at the border between these two divisions (Figure 13(b)). Immunostaining for PV is mostly absent in both divisions (Figure 13(c)), while a few palely stained CR-immunopositive neurons are observed in both divisions (Figure 13(e)), and the low density of OxA-immunopositive axons and bouton is similar in both divisions (Figure 13(f)). In contrast to this relative homogeneity of staining, CB immunostaining revealed a more complex organization. In both the SEd and SEv, CB immunostaining revealed a moderate density of neurons, but distinct core regions with pale CB neuropil immunoreactivity surrounded by a shell region with more intense CB neuropil immunoreactivity is observed (Figures 13(d), 14(b), and 14(d)). The intensity of CB neuropil immunoreactivity is higher in the SEds compared with the SEvs (Figures 13(d), 14(b), and 14(d)).

In addition to these distinct nuclei, two regions surrounding the tracts connecting the BNST to other parts of the brain we observed. We have termed these the lateral (PtRl) and medial (PtRm) para-tractal regions of the bed nucleus of the stria terminalis. The PtRl is a region that is located between the SEv and the rostral nuclear cluster (Figure 8d-u). The dorsal border of the PtRl is formed by the stria terminalis, while the commissural portion of the stria terminalis lies within the region (Figure 13). The neuronal density with the PtRl is lower than in adjacent nuclei (Figures 13a, 14e), while the myelin density is higher (Figure 13b). Immunostaining for PV, CR, and OxA was similar to adjacent nuclei (Figure 13c,e,f), as was the density of CB-immunopositive neurons, but there was a more intense CB neuropil immunoreactivity than in adjacent nuclei (Figures 13d, 14f). The PtRm was located on the ventromedial aspect of the rostral nuclear cluster, between the Pr and the BAC/stria medullaris (Figure 8k-m). Within the PtRm we noted a low neuronal density (Figure 10a), and low to moderate densities of CB- and CR-immunoreactive neurons (Figure 10c,d).

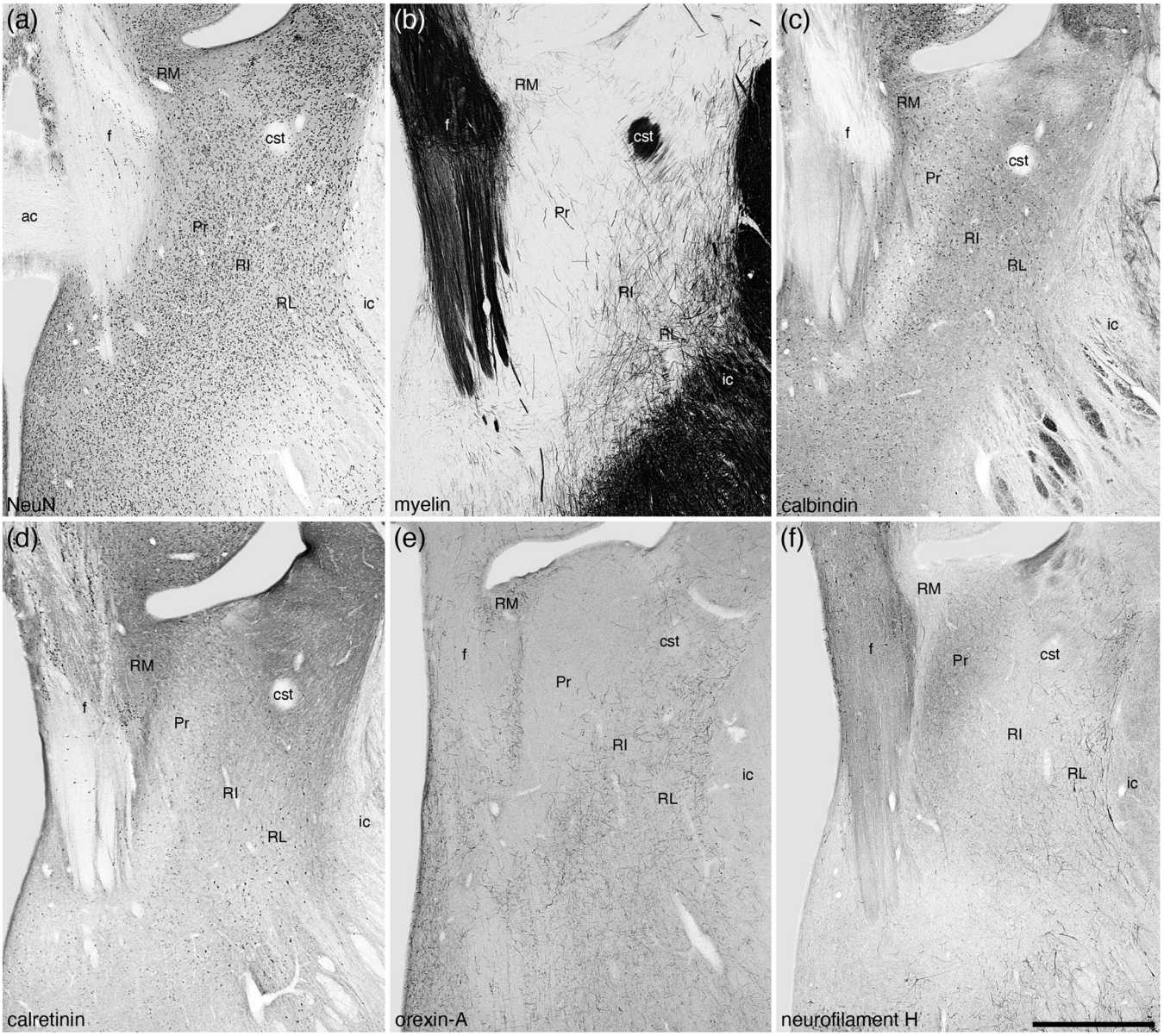

FIGURE 11 Low magnification photomicrographs of coronal sections through the tree pangolin brain showing the location of the nuclei forming the rostral portion of the bed nuclei of the stria terminalis including the rostral medial (RM), principal (Pr), rostral intermediate (RI), and rostral lateral (RL) divisions stained for neuronal nuclear marker (NeuN; a), myelin (b), calbindin (c), calretinin (d), orexin-A (e), and neurofilament H (f). Consistency in the variation of the patterns of staining allowed the delineation of these four nuclei, but we note here that the borders between the nuclei are not sharp, with the nuclei appearing to undergo transitions at their borders. In all images, medial is to the left and dorsal to the top. Scale bar in (f) = 1 mm and applies to all. See list for abbreviations

PV immunostaining revealed a moderate density of stained axons within this region (Figure 10b).

3.2 | Striatopallidal complex

3.2.1 | Ventral striatopallidal complex

The ventral striatopallidal complex, for the purpose of the current study, was considered to be composed of the Acb (core and shell), the olfactory tubercle, ventral parts of the caudate and putamen (see below), the ventral pallidum with the overlapping cholinergic neurons of the nucleus basalis (VP/N.Bas), the basal part of the substantia innominata (SIB), the lateral stripe of the striatum (LSS), the navicular nucleus (Nv), and the major island of Calleja (ICjM), all of which are located in positions relative to each other and the rest of the brain that could be described as typical of mammals (Figures 3, 15). A detailed description of the olfactory tubercle, and the minor islands of Calleja located within, of the tree pangolin has been provided previously (Imam et al., 2018a), and is not described further herein, but the location of these structures is depicted (Figure 3d-k).

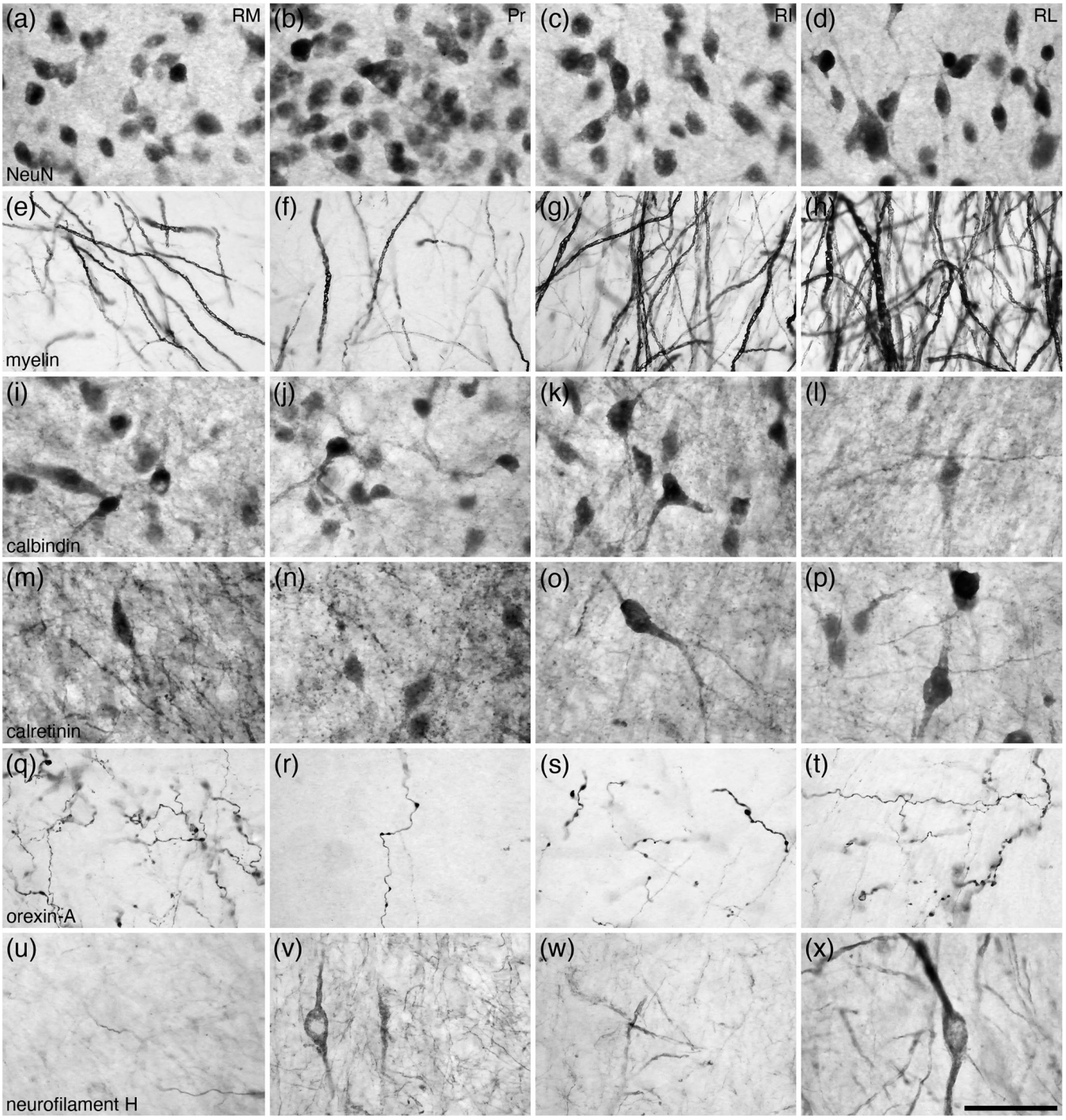

FIGURE 12 High magnification photomicrographs of coronal sections through the tree pangolin brain showing the architectural appearance of the nuclei forming the rostral portion of the bed nuclei of the stria terminalis, including the rostral medial (RM), principal (Pr), rostral intermediate (RI), and rostral lateral (RL) divisions stained for neuronal nuclear marker (NeuN; a–d), myelin (e–h), calbindin (i–l), calretinin (m–p), orexin-A (q–t), and neurofilament H (u–x). Note the variations in structural densities between the nuclei, which can be consistently employed to determine the extent of each of these nuclei. In all photomicrographs, medial is to the left and dorsal to the top. Scale bar in (x) = 50 μm and applies to all

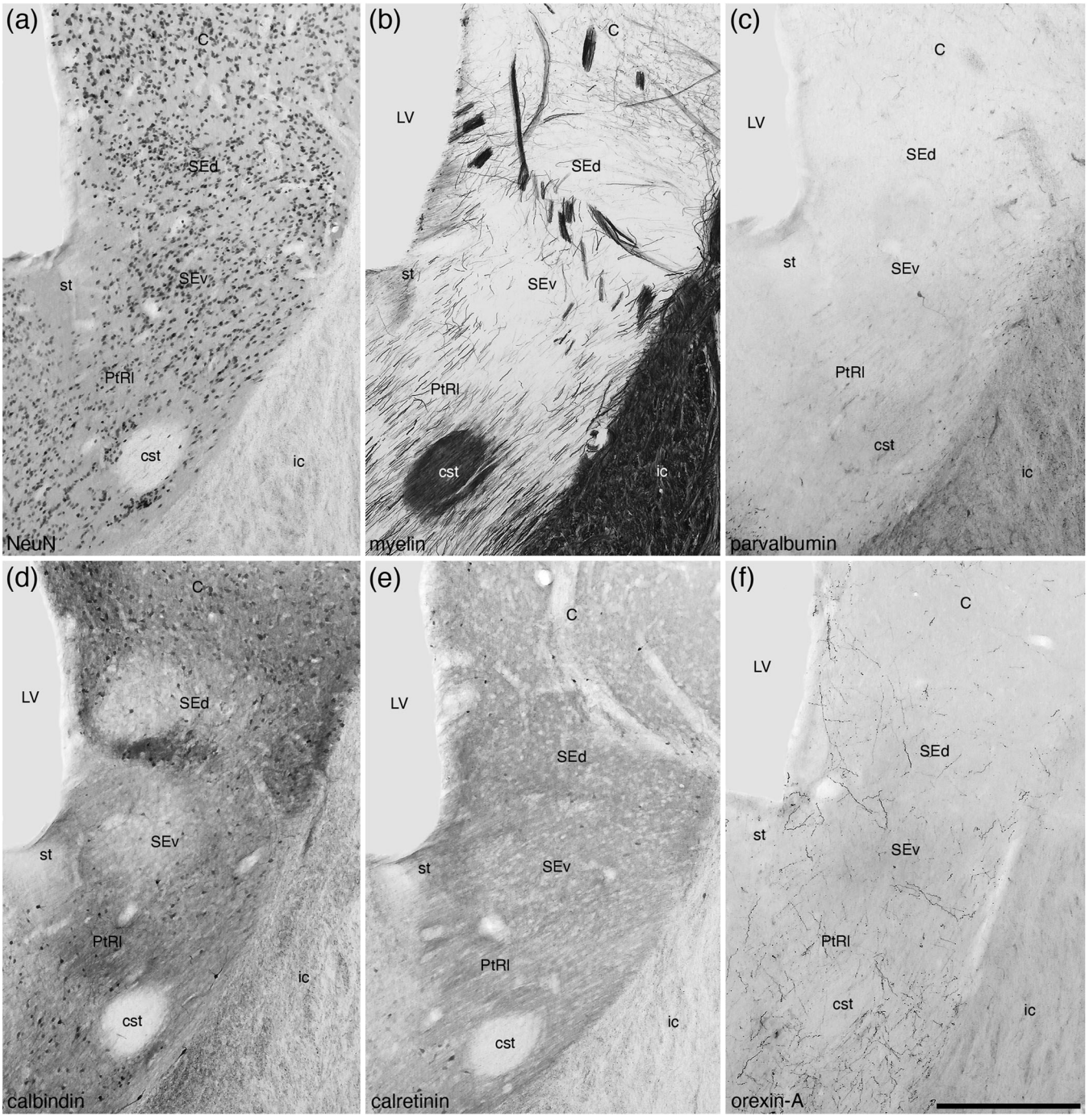

FIGURE 13 Low magnification photomicrographs of coronal sections through the striatal extension (SE) and lateral para-tractal region (PtRl) of the bed nuclei of the stria terminalis of the tree pangolin brain stained for neuronal nuclear marker (NeuN; a) myelin (b), parvalbumin (c), calbindin (d), calretinin (e), and orexin-A (f). Note the presence of both dorsal (SEd) and ventral (SEv) parts of the SE, which can be readily distinguished from each other and the PtRl with several of the stains employed in the current study. Calbindin staining (d) reveals a core (less intense staining) and surround (more intense staining) organization of the SEd and SEv. The lower neuronal density (a) and higher density of orexinergic terminals (f) in the PtRl distinguish this region, located around the stria terminalis (st) and the commissural stria terminalis (cst), distinguish this region from other parts of this nuclear complex. In all photomicrographs, medial is to the left and dorsal to the top. Scale bar in (f) = 500 μm and applies to all. See list for abbreviations

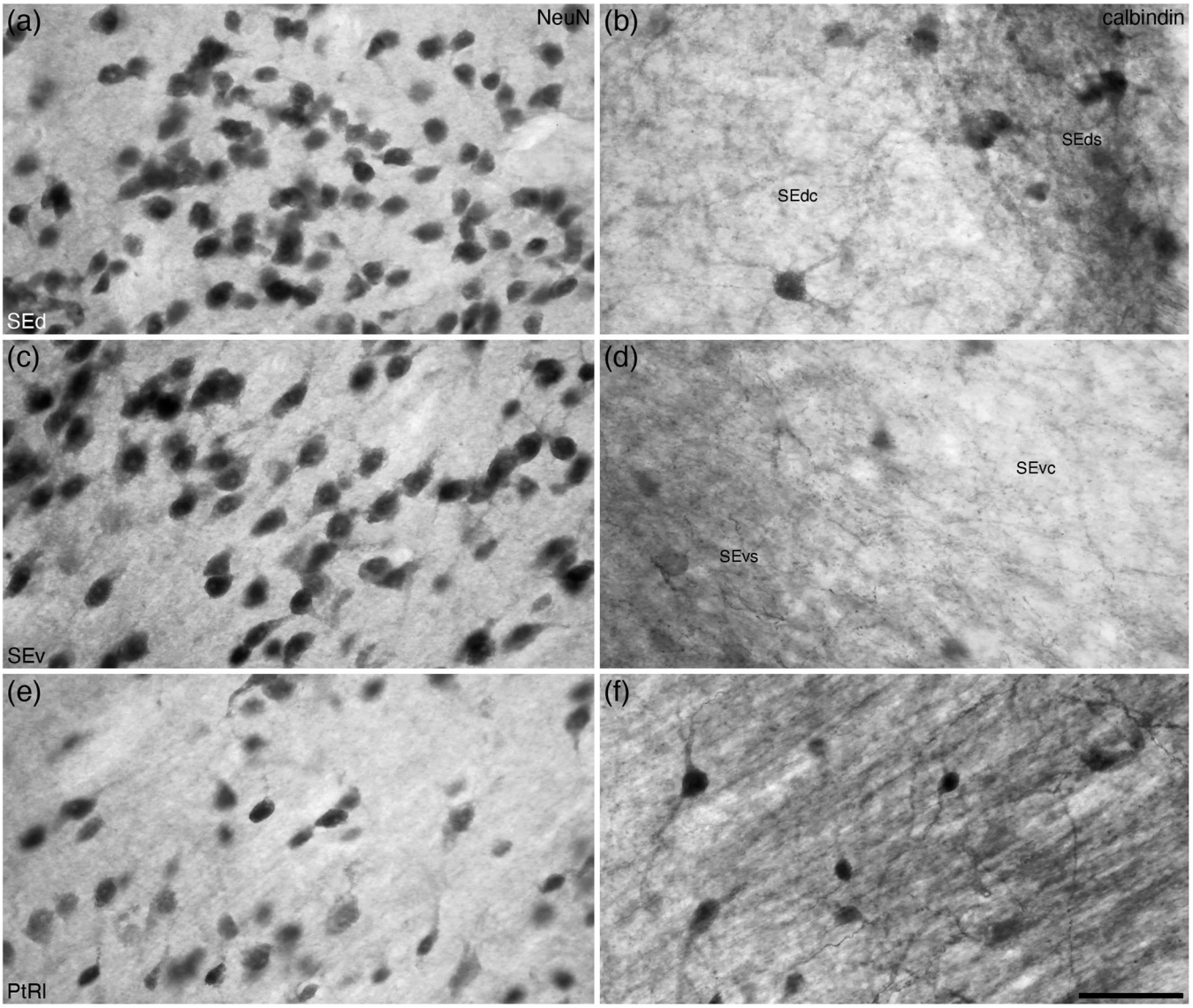

FIGURE 14 High magnification photomicrographs of coronal sections through the striatal extension (SE) and lateral para-tractal region (PtRl) of the bed nuclei of the stria terminalis of the tree pangolin brain stained for neuronal nuclear marker (NeuN; a, c, and e) and calbindin (b, d, and f). Note the presence of core (SEdc/SEvc) and surround (SEds/SEvs) subdivisions in both the dorsal (SEd) and ventral (SEv) parts of the SE, despite similar neuronal densities (a and c) in these regions. A greater density of calbindin immunopositive structures are observed in the SEds/SEvs compared with the SEdc/Sevc in both the Sed (b) and Sev (d). The lower neuronal density € and homogenous high density of calbindin immunopositive structures (f) in the PtRl distinguish this region from the SE. In all photomicrographs, medial is to the left and dorsal to the top. Scale bar in (f) = 50 μm and applies to all. See list for abbreviations

The nucleus accumbens (Acb) of the tree pangolin, composed of both core (AcbC) and shell (AcbSh) regions, was located in the ventral medial aspect of the telencephalon (Figures 3d-k, 15b-e, 16), as is typical across mammals. Throughout the Acb, a neuronal density similar to that observed in the caudate and putamen (see below) was observed (Figure 15, 16a, 17). The AcbSh spanned the medial and ventrolateral aspects of the AcbC, and a range of differences in the chemoarchitecture allowed us to delineate these two divisions of the Acb with reasonably certainty. The pattern of myelination is quite different between the AcbC and the AcbSh, with the AcbC showing distinct transected fascicles, while myelinated axons investing into the AcbSh showed a clearly different myelination pattern (Figures 16b, 18a). Many of these transected fascicles in the AcbC contained axons immunopositive to PV and NFH, whereas in the AcbSh, it appeared that the dendrites emanating from the ventral pallidum (see below), were immunopositive to these two markers (Figures 16e,h, 18b,e). While a moderate density of CB-immunopositive neurons were observed in both the AcbC and AcbSh, the AcbC evinced a more intense CB-immunostained terminal network than the AchSh (Figures 16f, 18c). In the AcbC, a moderate density of CR-immunopositive neurons was observed, but in the AcbSh the density of immunopositive neurons was substantially less (Figure 18d). The last significant

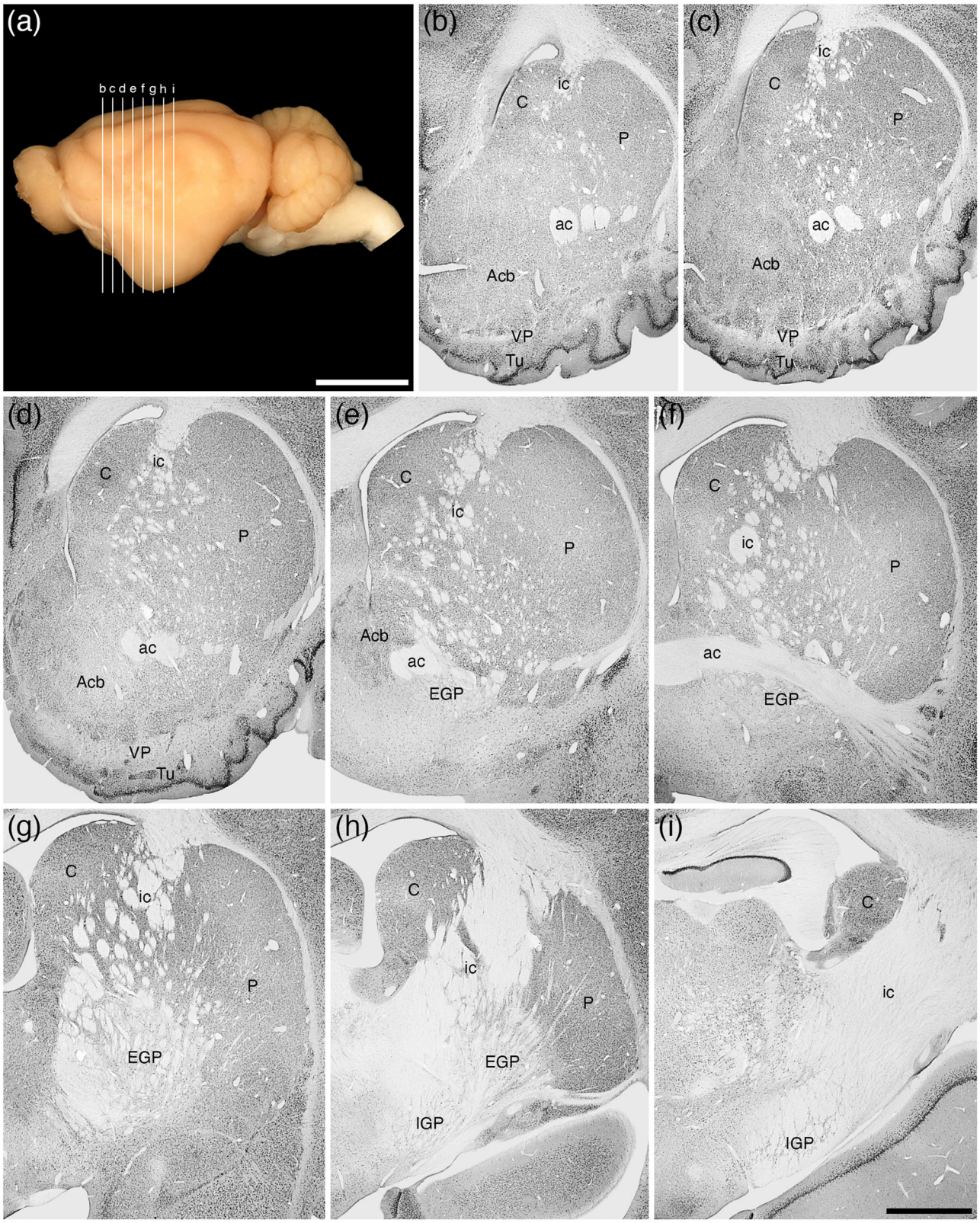

FIGURE 15 (a) Lateral view of the tree pangolin brain showing the levels at which the coronal sections imaged in (b)–(i) were taken. Scale bar in (a) = 1 cm and applies to (a) only. (b)–(i) A series of rostral to caudal low magnification photomicrographs of neuronal nuclear marker immunostained sections, each section being approximately 1000 μm apart. These images show the location of the components of the ventral striatopallidal complex, including the nucleus accumbens (Acb), the ventral pallidum (VP), and the olfactory tubercule (Tu), as well as the components of the dorsal striatopallidal complex, including the caudate nucleus (C), putamen nucleus (P), external globus pallidus (EGP), and internal globus pallidus (IGP; also referred to as the intrapeduncular or entopeduncular nucleus). Note that while the internal capsule (ic) is present, this pathway is only fully consolidated at the posterior aspects of the dorsal striatopallidal complex. In all photomicrographs, medial is to the left and dorsal to the top. Scale bar in (i) = 2 mm and applies to (b)–(i). See list for abbreviations

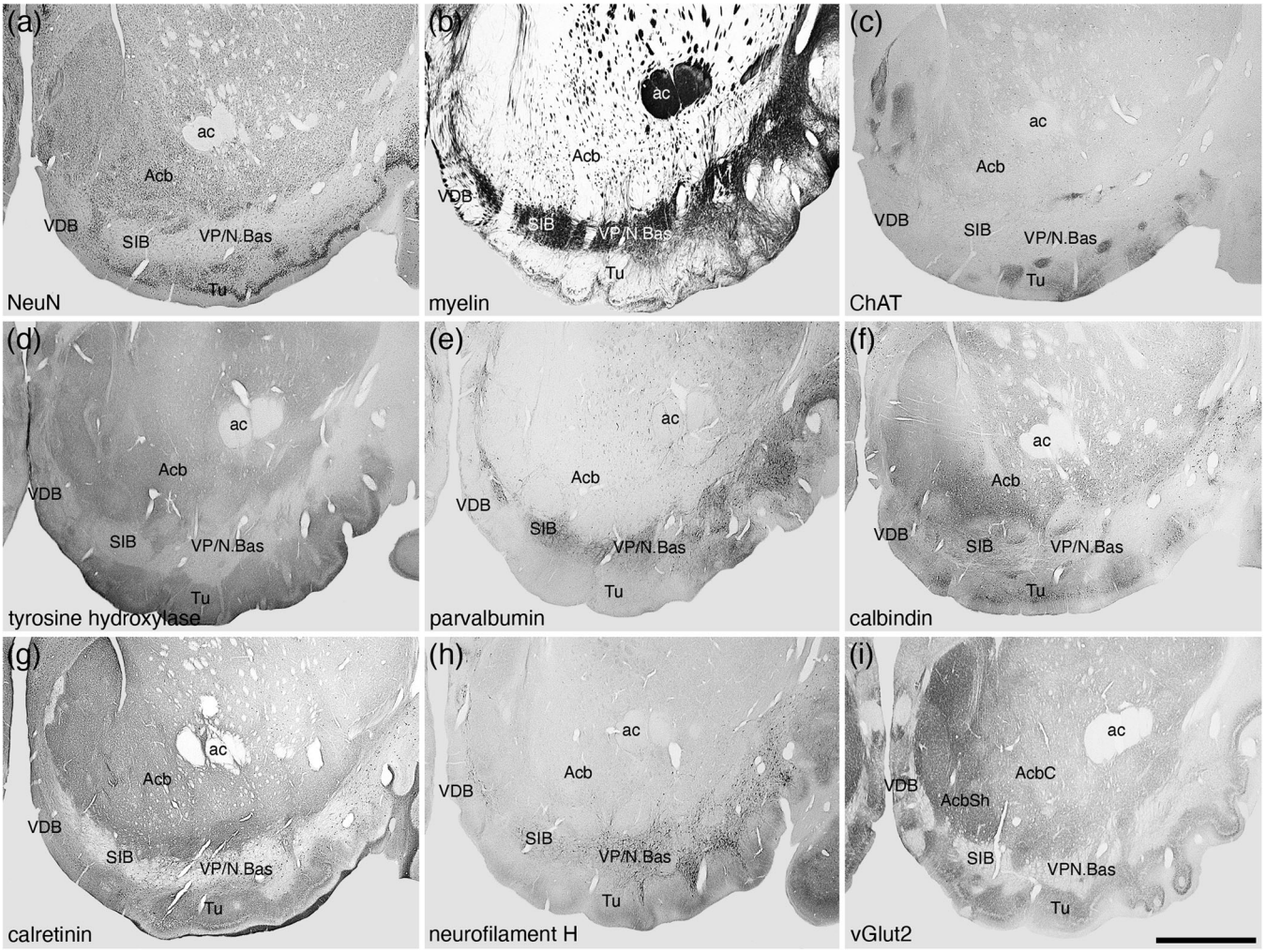

FIGURE 16 Low magnification photomicrographs showing the location of the nucleus accumbens (Acb), ventral pallidum (VP)/nucleus basalis (N.Bas), substantia innominata, basal part (SIB), vertical diagonal band (VDB), and olfactory tubercle (Tu) in coronal sections of the tree pangolin brain stained for neuronal nuclear marker (NeuN; a), myelin (b), choline acetyltransferase (ChAT; c), tyrosine hydroxylase (d), parvalbumin (e), calbindin (f), calretinin (g), neurofilament H (h), and vesicular glutamate transporter 2 (vGlut2; i), where the core (AcbC) and shell (AcbSh) are evident. Note that the VP/N.Bas and SIB are in a region of high myelin density (b) as well as a high density of parvalbumin (e) and neurofilament H (h) immunoreactive structures. The overlap of the cholinergic neurons of the N.Bas (c) with parvalbumin and neurofilament H immunoreactive structures has been used to delineate the VP, whereas the absence of cholinergic neurons is used to delineate the SIB. In all images, medial is to the left and dorsal to the top. Scale bar in (i) = 2 mm and applies to all. See list for abbreviations

difference between the AcbC and the AcbSh was the far higher density of vGlut2-immunopositive boutons in the AcbSh compared to the AcbC (Figure 18f,g). In addition to these variances between the AcbC and AcbSh, both evinced a moderate density of cholinergic neurons and a moderately intense terminal network immunopositive for TH (Figure 16d).

A cell sparse, densely myelinated band in apposition to the ventral border of the Acb and the dorsal border of the olfactory tubercle represents the regions where the ventral pallidum and the cholinergic neurons of the nucleus basalis (VP/N.Bas) and the basal part of the SIB is located (Figures 3 g-m, 16a,b, 17, 19a,b). Throughout this region, neurons immunopositive for PV, CB, CR, and NFH were evident (Figures 16e-h, 17c,d, 19d-f). In addition, this entire region evinced paler immunostaining for ChAT, TH, neuropil staining for CR, and vGlut2 (Figure 16c,d,g,i). Cholinergic neurons, presumably those of the N.Bas, were observed in the lateral two thirds of this region (Figures 3i-m, 17b, 19c).

The lateral stripe of the striatum (LSS) was located on the lateral margin of the Acb, nestled in the white matter between the Acb and the laterally located cortical and nuclear structures, rostral to the lateral portion of the posterior limb of the anterior commissure (Figures 3d-k, 20). A relatively high density of smaller neurons, plus the occasional larger neuron, were observed within the LSS (Figure 20a,b). Occasional cholinergic neurons, that have relatively larger soma, were observed in the LSS, as well as a high-density cholinergic terminal network (Figure 20c,d). Both larger and smaller neurons were seen to be PV-immunopositive, and a high-density PV-immunopositive terminal network was observed in the LSS (Figure 20e,f).

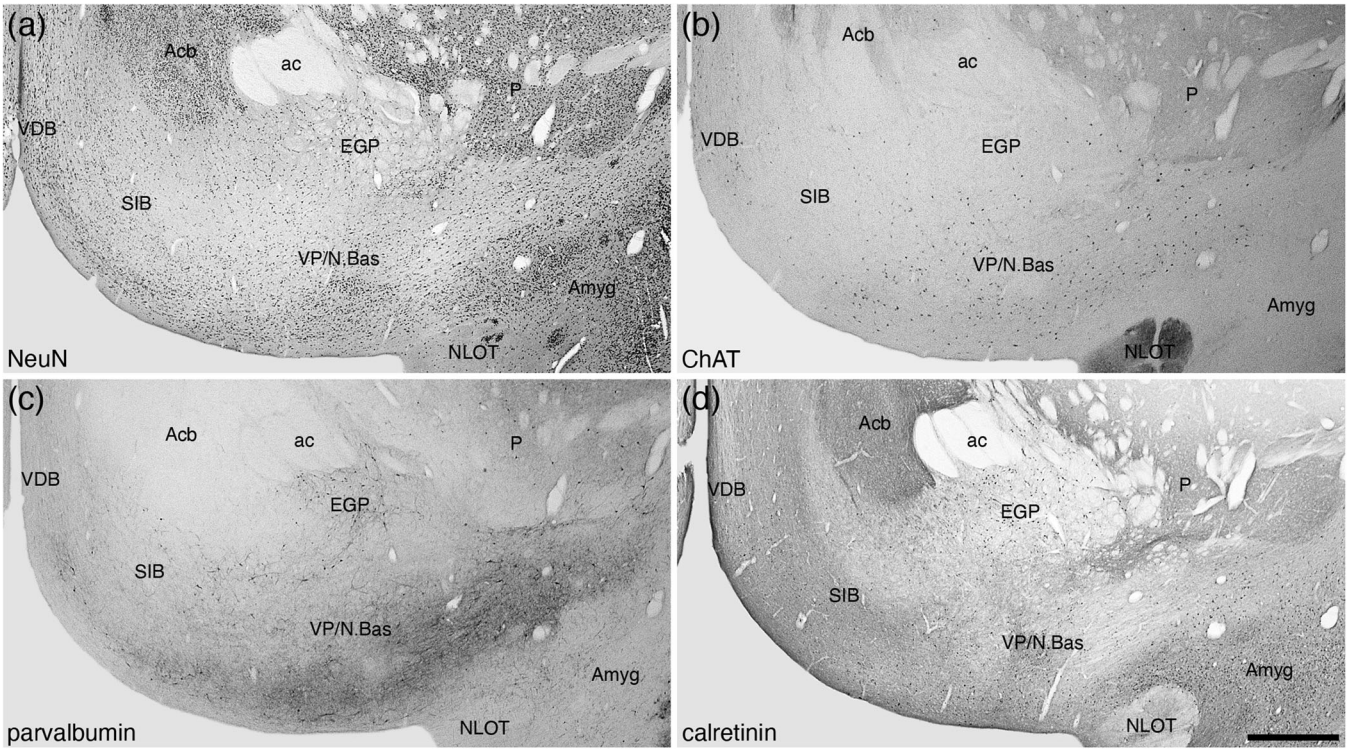

FIGURE 17 Photomicrographs of coronal sections through the ventral pallium/nucleus basalis (VP/N.Bas) of the tree pangolin brain stained for neuronal nuclear marker (NeuN; a), choline acetyltransferase (ChAT; b), parvalbumin (c), and calretinin (d). We have used the correlation of the presence of cholinergic neurons of the basal forebrain with other features to determine the location and extent of the VP/N.Bas and the substantia innominata, basal part (SIB), the SIB being the portion of this part of the brain that does not have cholinergic neurons of the N.Bas. In all photomicrographs, medial is to the left of the image and dorsal to the top. Scale bar in (d) = 1 mm and applies to all. See list for abbreviations

The small navicular nucleus of the basal forebrain was identified on the medial wall of the cerebral hemisphere, just rostral to the junction of the MS and the nucleus of the vertical limb of the diagonal band of Broca (Figure 3i, 21). Within the navicular nucleus, a moderate density of neurons and myelin fibers (Figure 21a) were observed, and small subset of neurons were PV- and CB-immunopositive (Figure 21b,c). The density of PV-, CB-, and vGlut2-immunopositive terminal networks was substantially lower than adjacent structures (Figure 21b-d), which allowed the accurate delineation of this nucleus.

The ICjM was located in the mediodorsal aspect of the shell of the accumbens nucleus (Figure 3 g-k) and was observed to be a high density of small, granular-shaped neurons (Figure 22a,b). A small number of the ICjM neurons were immunopositive for ChAT, CB, and CR (Figure 22c-e). A very intense ChAT-immunopositive terminal network was observed throughout the ICjM, but the intensity of CB, CR, and vGlut2 immunolabeled terminal networks was substantially lower than the adjacent structures (Figure 22c-f).

3.2.2 | Dorsal striatopallidal complex

Within the dorsal striatopallidal complex, we include the caudate/putamen, and the external and internal globus pallidus. The caudate and putamen occupy a position within the telencephalon of the tree pangolin similar to that observed in other mammals (see Figures 5 and 6 of Imam et al., 2017; and Figures 1, 3, 8, 15, 23). Rostrally, the neurons forming the caudate and putamen are contiguous (Figure 15b-d). In the more caudal aspects of these nuclei, the fasciculi of the internal capsule consolidate to separate these two nuclei (Figure 15e-h). Throughout the caudate/putamen, a moderate to high density of neurons was observed (Figure 15). Subsets of the caudate/putamen neurons were immunoreactive to PV (Figure 23a), CR (Figure 23c), ChAT (Figure 23d), with scattered larger neurons being NFH immunopositive. CB immunostaining revealed the presence of a higher density of immunoreactive neurons of two types, a larger, multipolar, intensely immunoreactive neuronal type, and a smaller, multipolar, weakly immunoreactive type (Figure 23b). Immunostaining for ChAT (Figure 23d), TH (Figure 24c), and vGlut2 revealed moderately dense terminal networks throughout both the caudate and a putamen.

Both the external (EGP) and internal (IGP) globus pallidi were readily identified in the tree pangolin brain, occupying a position in relation to other structures that could be considered quite typical for mammals (Figures 3k-m, 8d-l, 15e-i). The density of neurons within both EGP and IGP was substantially lower than in the caudate/putamen (Figure 15e-i), but both had much higher densities of myelinated fibers (Figure 24a). The vast majority of EGP neurons were immunopositive for PV (Figures 23e, 24b,e), CR (Figure 23f), and

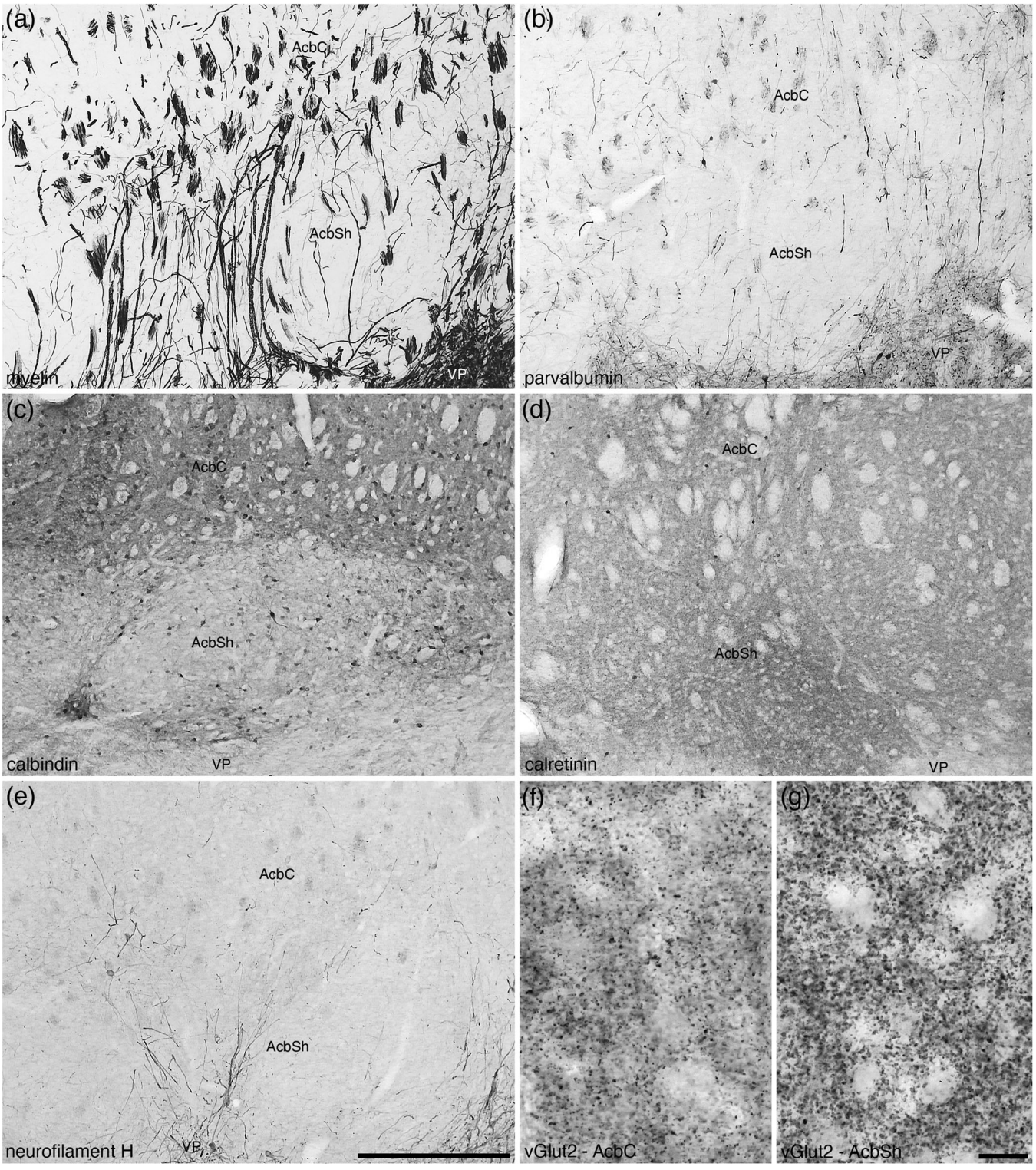

FIGURE 18 Photomicrographs of coronal sections from the brain of the tree pangolin detailing the subtle myeloarchitectural (a) and chemoarchitectural (b–g) differences between the core (AcbC) and shell (AcbSh) regions of the nucleus accumbens. The sections depicted here were stained for myelin (a), parvalbumin (b), calbindin (c), calretinin (d), neurofilament H (e), and vesicular glutamate transporter 2 (vGlut2; f and g). While the border between the AcbC and AcbSh is best considered to be a gradient of variation, we could observe substantive differences. Axonal staining for myelin (a), parvalbumin (b), and neurofilament H (e) show a greater number of cross-sectional axonal profiles in the AcbC compared with the longitudinal profiles observed in AcbSh. The AcbC exhibits a higher intensity neuropil staining for calbindin than the AcbSh (c), while the AchSh exhibits a lower density of calretinin immunopositive neurons than the AcbC (d). The density of vGlut2 immunopositive boutons is lower in the AcbC (f) when compared with the AcbSh (g). In all photomicrographs, medial is to the left of the image and dorsal to the top. Scale bar in (e) = 500 μm and applies to (a)–(e). Scale bar in (g) = 20 μm and applies to (f) and (g). See list for abbreviations

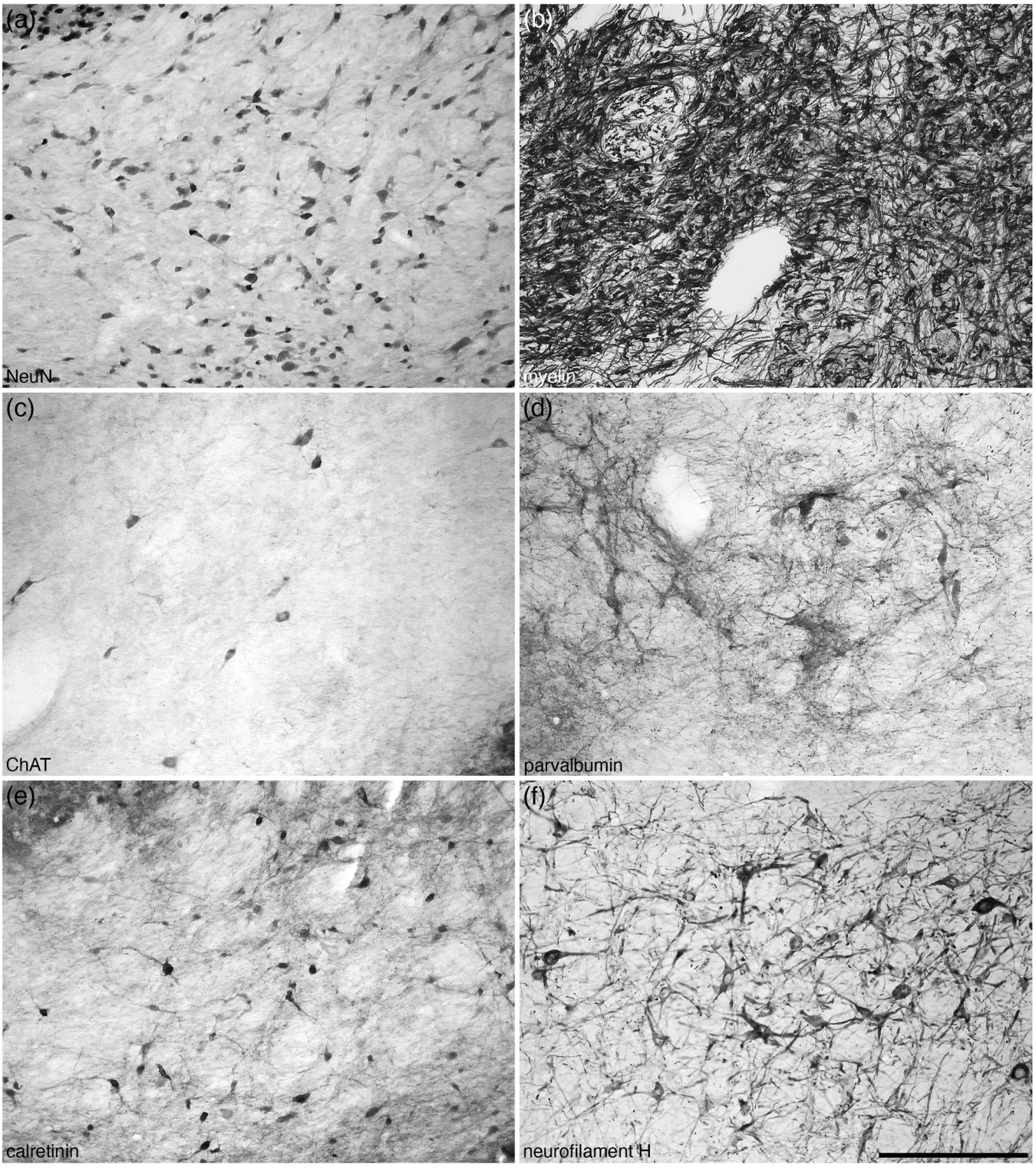

FIGURE 19 Photomicrographs of coronal sections through the ventral pallium/nucleus basalis of the tree pangolin brain stained for neuronal nuclear marker (NeuN; a), myelin (b), choline acetyltransferase (ChAT; c), parvalbumin (d), calretinin (e), and neurofilament H (f). Note that in this heavily myelinated region (b), a low density of neurons is observed (a), some of which are cholinergic (c), and others that contain calretinin (e). Immunostaining for parvalbumin (d) and neurofilament H (f) reveal a high density of different neural structures in this region of the brain. In all photomicrographs, medial is to the left of the image and dorsal to the top. Scale bar in (f) = 250 μm and applies to all

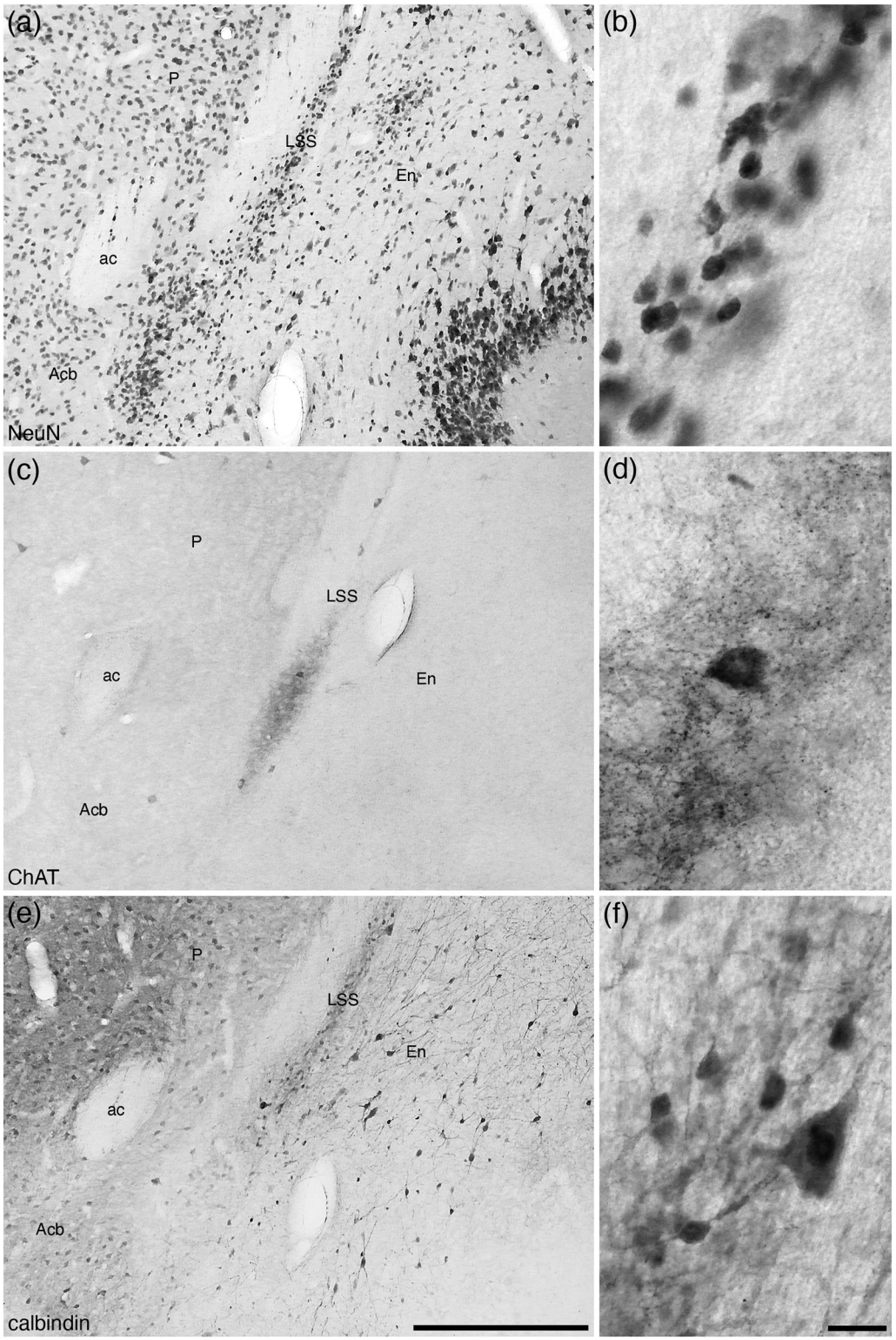

FIGURE 20 Low (a, c, and e) and higher (b, d, and f) magnification photomicrographs of coronal sections through the lateral stripe of the striatum (LSS), part of the ventral striatopallidal complex, of the tree pangolin brain immunostained for neuronal nuclear marker (NeuN; a and b), choline acetyltransferase (ChAT; c and d) and calbindin (e and f). The LSS is found in the white matter lateral to the putamen (P) and nucleus accumbens (Acb) and medial to the endopeduncular nucleus (En). A small number of cholinergic neurons and dense cholinergic bouton densities are observed in the LSS (d), as well as two different sized calbindin immunopositive neurons (f). In all photomicrographs, medial is to the left and dorsal to the top. Scale bar in (e) = 500 μm and applies to (a), (c), and (e). Scale bar in (f) = 20 μm and applies to (b), (d), and (f). See list for abbreviations

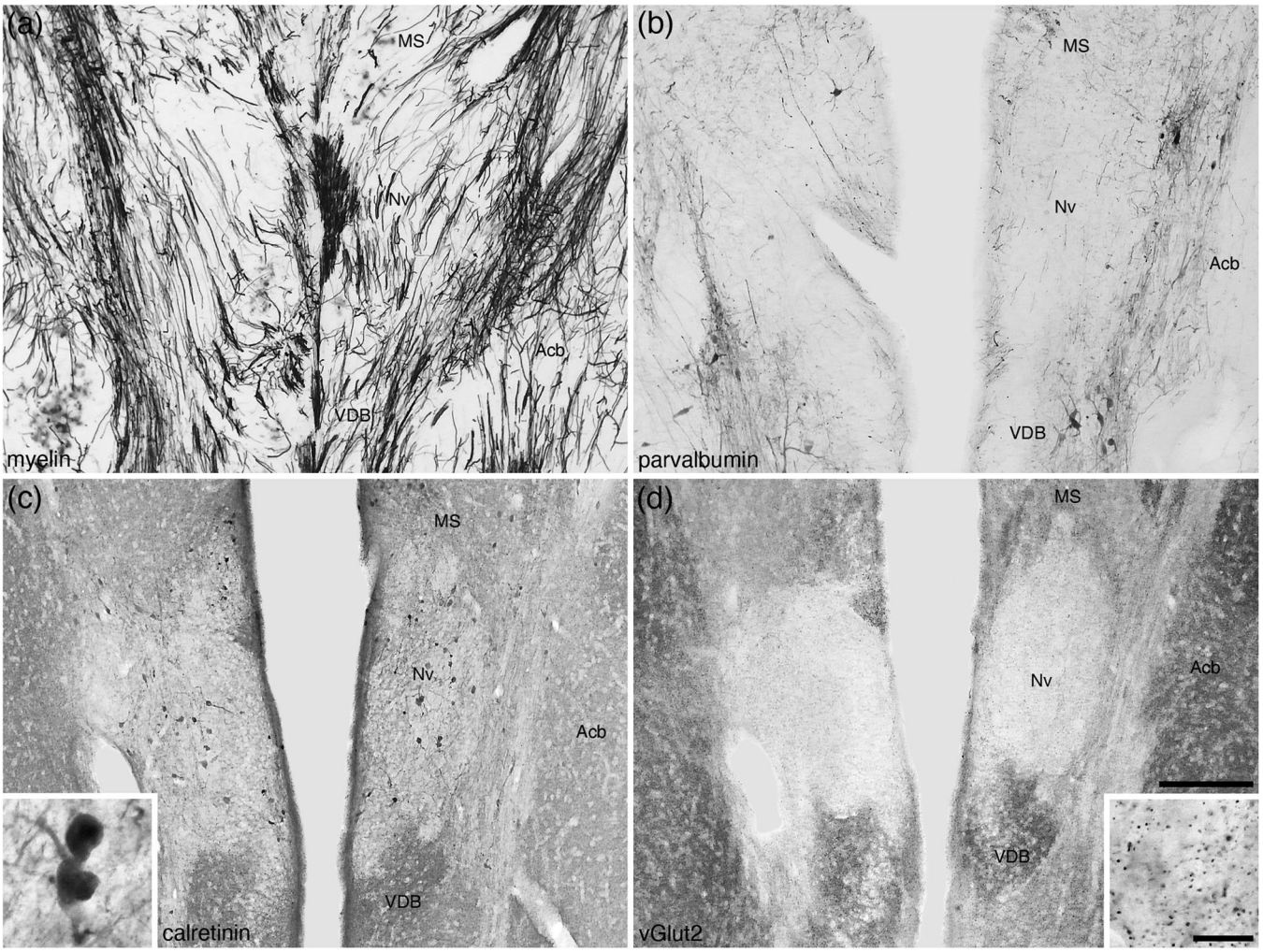

FIGURE 21 Low (a–d) and higher (insets c and d) magnification photomicrographs of coronal sections through the navicular nucleus of the basal forebrain (Nv) of the tree pangolin brain stained for myelin (a), parvalbumin (b), calretinin (c), and vesicular glutamate transporter 2 (vGlut2; d). Note the pale neuropil staining for parvalbumin (b), calretinin (c), and vGlut2 (d) that delineate this nucleus from the medial septal nucleus (MS) dorsally, the vertical diagonal band (VDB) ventrally and the nucleus accumbens (Acb) laterally. A low density of calretinin immunopositive neurons are observed in the Nv (c) as well as a low density of vGlut2 immunopositive boutons (d). In all photomicrographs, medial is at the center of the image and dorsal to the top. Scale bar in (d) = 250 μm and applies to all. Scale bar in inset (d) = 20 μm and applies to both insets. See list for abbreviations

NFH (Figures 23h, 24d,f). Scattered CB-immunopositive and cholinergic neurons were observed around the lateral, dorsal and ventral borders of the EGP (Figures 3k-m, 23 g), but no significant terminal network immunopositive for ChAT was observed. A low to moderate density of TH-immunopositive fibers (Figure 24c) and a very low-density vGlut2 terminal network were observed. The vast majority of IGP neurons evinced immunoreactivity to PV (Figure 24b,e), CR, and NFH (Figures 23i, 24d,f). A very low-density vGlut2 terminal network was observed in the IGP, with a moderate to high density of TH-immunopositive fibers being present (Figure 24c). No structures within the IGP showed immunoreactivity for CB or ChAT.

4 | DISCUSSION

The current study provides a description of the cyto-, myelo-, and chemoarchitecture of the subpallial telencephalon of the tree pangolin. While the individual nuclei that constitute the subpallium are not disputed (e.g., Watson et al., 2017), how these are arranged into various morpho-functional and developmental groupings, units, or circuits is still discussed, including the assignation of the portions of the extended amygdala (e.g., Alheid, 2003; de Olmos et al., 2004) and the basal forebrain cholinergic neurons (e.g., Geula et al., 2021). We have organized our description based on the division of the subpallium into a septal region following Risold (2004) and the striatopallidal complex

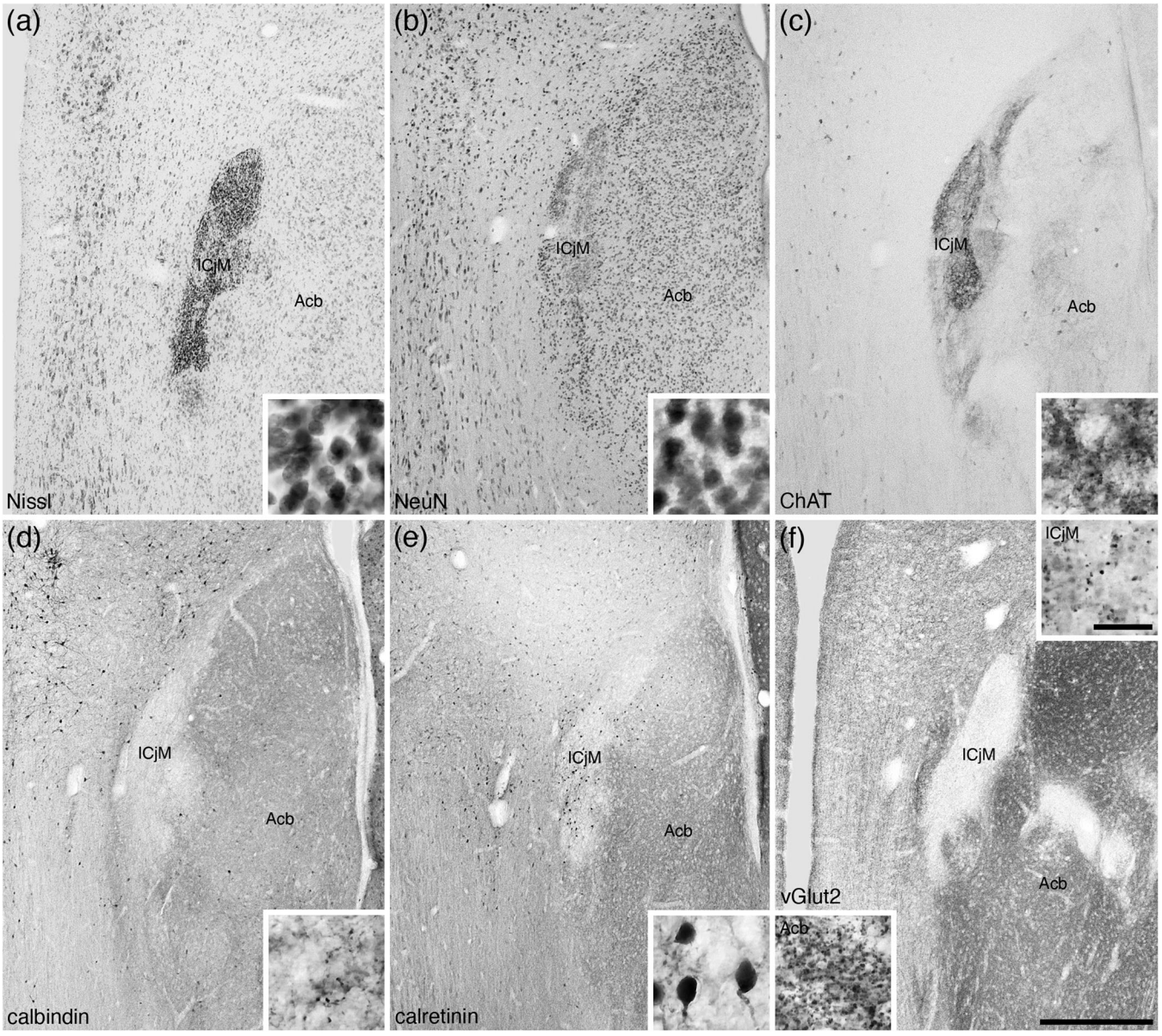

FIGURE 22 Low (a–f) and higher (insets a–f) magnification photomicrographs of coronal sections through the major Island of Calleja (ICjM) of the tree pangolin brain stained for Nissl (a), neuronal nuclear marker (NeuN; b), choline acetyltransferase (ChAT; c), calbindin (d), calretinin (e), and vesicular glutamate transporter 2 (vGlut2; f). Note the high density of small neurons forming the ICjM (a and b), some of which are calretinin immunopositive (e). A high density of ChAT immunopositive boutons (c) and lower densities of calbindin (d) and vGlut2 (f) boutons. A high density of vGlut2 boutons was observed in the adjacent nucleus accumbens (Acb; f). In all photomicrographs, medial is to the left and dorsal to the top. Scale bar in (f) = 500 μm and applies to all. Scale bar in inset (f) = 20 μm and applies to all insets. See list for abbreviations

following Chen et al. (2020); however, the septal region of Risold (2004) contains both the septal nuclear complex and the BNST, while the striatopallidal complex of Chen et al. (2020) is composed of both ventral and dorsal portions. Given that there are varied functional emphases for each these regions, we discuss the septal nuclear complex and diagonal band of Broca, the BNST, and the ventral and dorsal portions of the striatopallidal, as separate entities to allow us to determine whether any specific chemoarchitectural variations of these entities in the tree pangolin have functional implications related to the life history of the tree pangolin.

4.1 | Septal nuclear complex

The septal nuclear complex is often parcellated into four groups, several of which are divided into multiple nuclei, as well as the diagonal band of Broca (vertical and horizontal limbs, Ch2 and Ch3, respectively, of Geula et al., 2021); however, detailed architectonic and hodological studies reveal a far more complex organization of this subpallial region (e.g., Risold & Swanson, 1997; Paxinos et al., 2009; Radtke-Schuller, 2018). Our analysis of the septal nuclear complex in the tree pangolin revealed both a regional and nuclear organization very similar to that

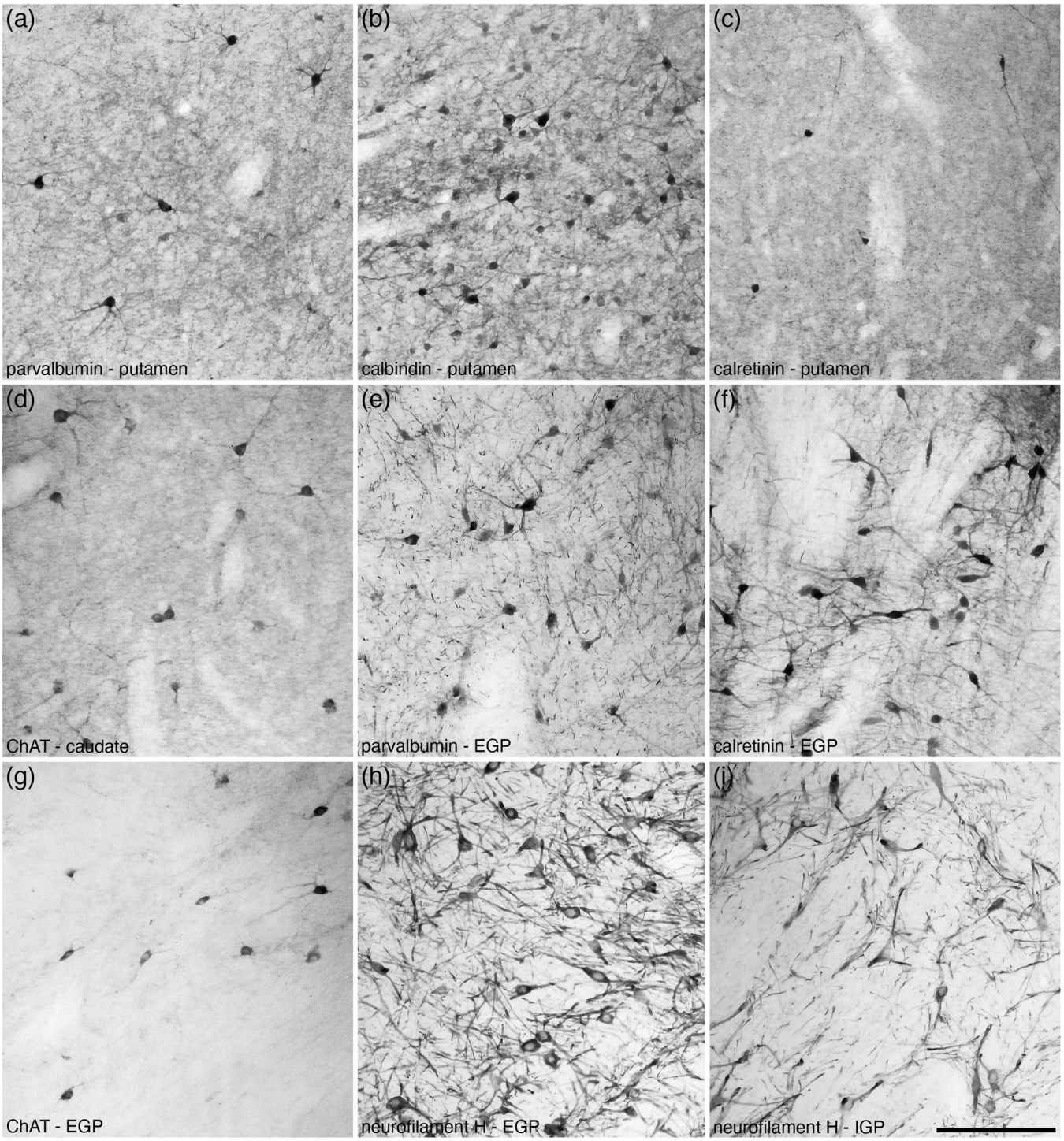

FIGURE 23 High magnification photomicrographs of coronal sections through the dorsal striatopallidal complex of the tree pangolin brain immunostained for parvalbumin (a and e), calbindin (b), calretinin (c and f), choline acetyltransferase (ChAT; d and g) and neurofilament H (h and i). These images show examples of the relative density and neuronal morphology of immunopositive neurons and other structures in the putamen (a–c), caudate (d), external globus pallidus (EGP; e–h) and the internal globus pallidus (IGP; i). In all photomicrographs medial is to the left and dorsal to the top. Scale bar in (i) = 200 μm and applies to all

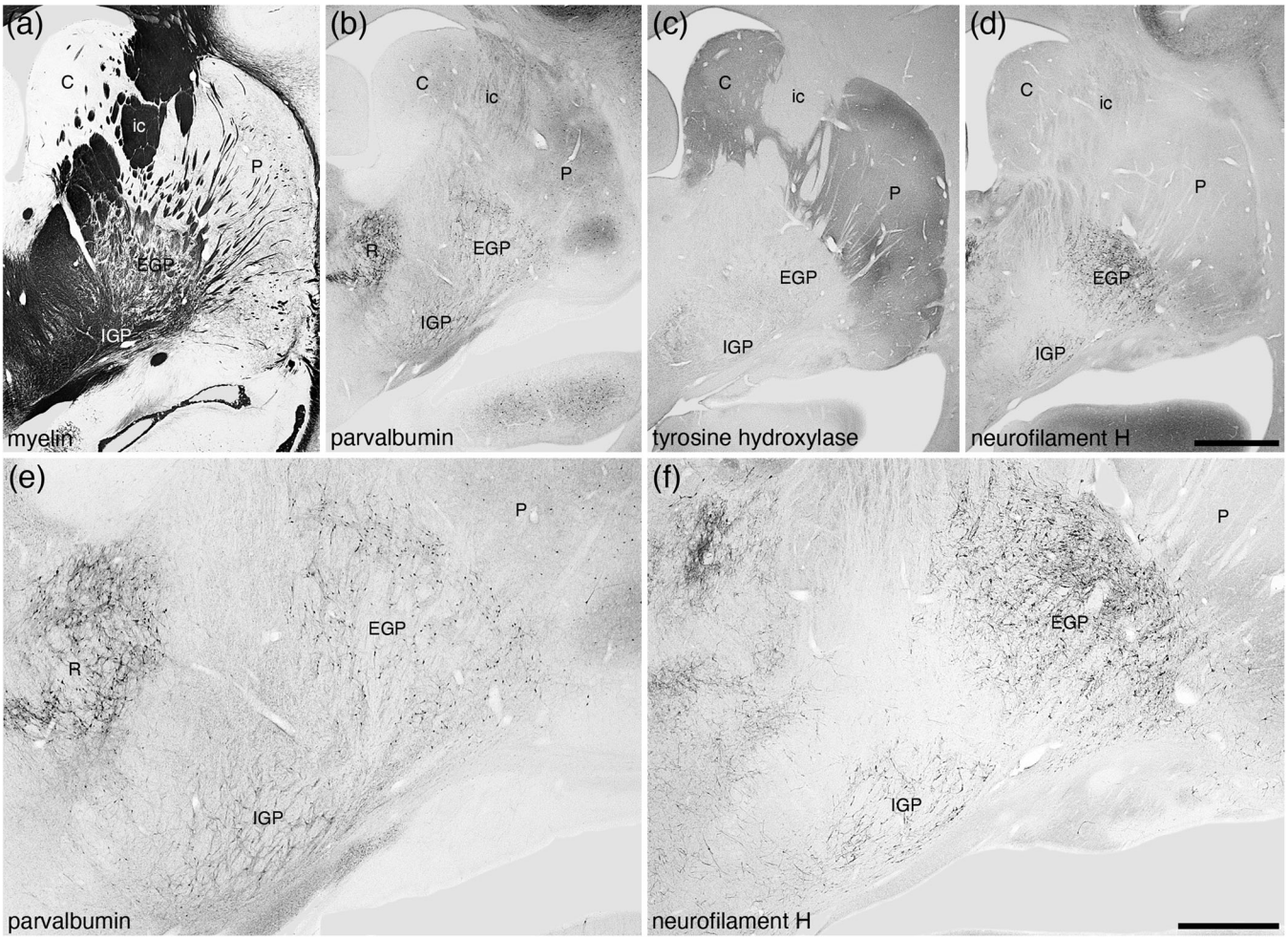

FIGURE 24 Low magnification photomicrographs of coronal sections through the dorsal striatopallidal complex of the tree pangolin brain stained for myelin (a), parvalbumin (b and e), tyrosine hydroxylase (c), and neurofilament H (d and f). These images demonstrate the location of the components of this complex including the caudate nucleus (C), putamen nucleus (P), external globus pallidus (EGP), internal globus pallidus (IGP), and the internal capsule (ic). Panels (e) and (f) show higher magnification images of the EGP and IGP stained for parvalbumin (e) and neurofilament H (f), which clearly demonstrate these nuclei. In all photomicrographs medial is to the left and dorsal to the top. Scale bar in (d) = 2 mm and applies to (a)–(d). Scale bar in (f) = 1 mm and applies to (e) and (f). See list for abbreviations

observed in the laboratory rat (e.g., Risold & Swanson, 1997; Paxinos et al., 2009) and domestic ferret (Radtke-Schuller, 2018). No readily observable major differences were noted, apart from slight variations in the relative size of different nuclei. Interestingly, in addition to the topographical location, the vertical and horizontal limbs of the diagonal band of Broca could be reliably parcellated based on the presence of CB-immunopositive neurons with larger soma in the horizontal limb compared with the vertical limb.

The lateral aspect of the septum, which contains a large number of individual nuclei, appears to play a central role in the incorporation of movement during the evaluation of stimuli in the current environment and how this relates to current motivation, anxiety and reward, providing an assessment of what has been termed by Wirtshafter and Wilson (2021) as the "integrated movement value signal." The MS (which is partly composed of cholinergic neurons, the Ch1 of Geula et al., 2021), is known to be involved in locomotion, the generation of the theta rhythm in the hippocampus, and is also be involved in the motivation of undertaking actions (Mocellin & Mikulovic, 2021). The diagonal band of Broca is thought to be involved in memory retrieval (Liu & Gentleman, 2021) through the action of its projections upon the hippocampal formation (Roland et al., 2014). It would be reasonable to assume, given the overall similarities between the organization of the septal nuclear complex and diagonal band of Broca, and the tree pangolin hippocampal formation (Imam et al., 2019a), to other mammals, that the functional role/s of the septal nuclear complex and diagonal band in the tree pangolin are likely to be very similar to that observed in other mammals; however, what environmental signals play a role in the activation of septal neurons in the tree pangolin may be quite different to that in, for example, the laboratory rat.

4.2 | Bed nuclei of the stria terminalis

Detailed architectural analyses of the BNST are mostly restricted to the laboratory rodent, although the precise architectural borders and

nomenclature differ even within this species (e.g., Ju & Swanson, 1989; Paxinos et al., 2009), with analyses in other mammal species usually providing broad nuclear/regional subdivisions (e.g., Radtke-Schuller, 2018). Our analysis of the BNST in the tree pangolin resembles that provided in the laboratory rodent, although two substantive variations were noted. The first variation concerns what we term the main nuclear cluster, which is composed of four nuclei that form adjacent parallel laminae. Based on the architectonic appearance, one of these nuclei is likely to be homologous to the principal nucleus of Ju and Swanson (1989), the name that we assign to this nucleus. The principal nucleus, as defined by Ju & Swanson and used herein, appears to belong to the medial division of Paxinos et al. (2009). The organization of these nuclei in the main cluster is reminiscent of that reported in the rodent, but in the rodent, these nuclei have been subdivided into anterior and posterior parts, which with the range of stains used in the current study were not readily observable. The parcellation of this region of the BNST also includes separate nuclei around the anterior commissure, but our analysis did not indicate any heterogeneity in the cyto-, myelo-, or chemoarchitecture, that would have permitted reliable delineate of these parts, although the appearance of the named nuclei in the tree pangolin around the anterior commissure bear a striking resemblance to that observed in the laboratory rat. Thus, while we acknowledge the potential for further parcellation of the nuclei, and potential nomenclature reconciliation, within the main cluster of the BNST of the tree pangolin, we were unable to reveal them in the current study. There are two possibilities to explain this, first, that alternative stains to those used in the current study may reveal additional divisions of these nuclei, or second, that the tree pangolin has a simpler organization of these nuclei than that of the laboratory rat.

The second difference noted to the laboratory rodent was the presence of a distinct, and seemingly complexly organized, striatal extension of the bed nucleus of the stria terminalis. The striatal extension, a single nucleus, is described in the laboratory rat by Ju and Swanson (1989) and appears to correspond to the two subdivisions of the supracapsular division of Paxinos et al. (2009). While this is a relatively small region in the laboratory rat, in the tree pangolin, we noted two distinct divisions of this region, dorsal and ventral, with both of these divisions being composed of a core and shell region. Thus, in comparison with the laboratory rat, the striatal extension of the BNST within the tree pangolin appears to have a more complex organization. This may reflect a true difference in complexity, or this core and shell organization of the striatal extension may not have yet been observed in the laboratory rat, as this organization was most evident with CB immunostaining. If this region of the BNST is indeed more complexly organized in the tree pangolin compared with the laboratory rat, this indicates that it is possible that the neural processing that occurs in this region is also more complex. While the striatal extension is connected with other nuclei within the BNST (e.g., Dong & Swanson, 2004), no specific study of the connectivity or function of the striatal extension, to our knowledge, has been undertaken, making any specified functional interpretation untenable at present.

The BNST have been associated with a wide range of functions, these studies being undertaken primarily in laboratory rodents and humans. Proposed functions include slower-onset, longer lasting responses related to fear, stress, and anxiety (Walker et al., 2003; Somerville et al., 2010), modulation of the hypothalamic–pituitary–adrenal axis by the anteroventral nuclei (Radley & Johnson, 2018), regulation of ingestive behaviors by the rhomboid nucleus (Dong & Swanson, 2003), control of social defensive and reproductive behaviors by the posterior nuclei (Dong & Swanson, 2004), and control of autonomic and neuroendocrine functions (Crestani et al., 2013). Despite the differences noted in the organization of this nuclear complex in the tree pangolin, it would be reasonable to assume that these functions are applicable to the BNST of the tree pangolin, and that only minor variations on these broad functional attributes of this intricate nuclear may be present in the tree pangolin.

4.3 | Ventral striatopallidal complex

In the current study, we defined the ventral striatopallidal complex as being composed of the Acb (core and shell), the olfactory tubercle, the ventral pallidum, the cholinergic neurons of the nucleus basalis, the basal part of the SIB, the lateral stripe of the striatum, the navicular nucleus, and the major island of Calleja. The location, cyto-, myelo-, and chemoarchitecture of these nuclei, with the range of stains used in the current study indicate that the organization of this region of the tree pangolin brain is similar to that of other mammals (e.g., Paxinos et al., 2009; Pillay et al., 2017; Radtke-Schuller, 2018). One area of uncertainty we encountered regards the precise definition, or overlap, of the ventral pallidum, the nucleus basalis (Ch4 of Geula et al., 2021), and the basal part of the SIB. These three nuclei/regions lie between the ventral border of the Acb and the dorsal border of the olfactory tubercle. The nucleus basalis is typically identified as being composed of cholinergic neurons (Geula et al., 2021), which is the criteria we used in this study, whereas the cyto-, myelo-, and chemoarchitectures of the ventral pallidum and the SIB, with the range of stains used in the current study, were quite similar, both being neuron sparse, myelin dense, absent to low TH immunoreactivity, extensive PV and NFH-immunopositive networks of cells and dendrites, and both containing many CR-immunopositive neurons. The distinction that we used to delineate the extent of ventral pallidum and the SIB, and that resembles that provided in atlases of the rat brain (Paxinos et al., 2009), was the presence of the cholinergic neurons of the nucleus basalis, which we have used as a marker to delineate the ventral pallidum, the SIB being devoid of these cholinergic neurons; however, our definition must be used cautiously, as it appears that the cholinergic neurons of the nucleus basalis are often thought to overlap with the SIB, although in these cases no mention of the ventral pallidum is made (e.g., Colloby et al., 2016).

The structures of the ventral striatopallidal complex are involved in a range of functions. The Acb (both core and shell to differing degrees) appears to be a neural interface balancing and regulating biological drives related to survival and reproduction (e.g., Salgado & Kaplitt, 2015) and play a significant role in the modulation of social behaviors (e.g., Ploeger et al., 1991; Manduca et al., 2016 . The olfactory tubercle

is thought to be involved in odor-guided motivation and the regulation of eating behaviors (e.g., Murata, 2020). The ventral pallidum and SIB play major roles in the encoding and enhancement of reward and motivation (e.g., Smith et al., 2009), while the overlapping cholinergic neurons of the nucleus basalis play a role in attention control and the maintenance of arousal (e.g., Koulousakis et al., 2019). A specific function/s for the lateral stripe of the striatum does not appear to have been determined, although it is known that these neurons produce preprotachykinin B and project to the SIB and other regions of the basal forebrain (Zhou et al., 2004). Similarly, specific functions for the navicular nucleus and the major island of Calleja are not clear, although it would seem likely that they play a role in the neural reward system. Given the overall similarity, in terms of cyto-, myelo-, and chemoarchitecture of the ventral striatopallidal complex in the tree pangolin to that seen in other mammalian species, it would be reasonable to conclude that the functions associated with these nuclei are also likely to be similar, although perhaps driven by species-specific stimuli relevant to the tree pangolin.

4.4 | Dorsal striatopallidal complex

The dorsal striatum is considered to be composed of the caudate/putamen nuclei, along with the internal and external divisions of the globus pallidus (e.g., Mai & Ashwell, 2004; Chen et al., 2020). These nuclei could be readily identified in the tree pangolin and it should be noted that the internal globus pallidus is synonymous with the endopeduncular nucleus. In the tree pangolin, a distinct internal capsule demarcating the caudate and putamen nuclei in their caudal aspects is present, a feature shared with closely related species (e.g., the ferret, Radtke-Schuller, 2018). In addition, the chemical neuroanatomy of these nuclei, with features such as the presence of cholinergic interneurons in the caudate and putamen, the dense dopaminergic innervation of the caudate and putamen revealed with TH immunostaining, and the PV-immunopositive staining of all neurons in the external and internal globus pallidus, being generally associated with these nuclei across mammal species (e.g., Lanciego et al., 2012). Add to this, the presence of a subthalamic nucleus (Imam et al., 2019b), portions of the dorsal thalamus (Imam et al., 2019b), and the substantia nigra (Imam et al., 2019c), makes it is reasonable to conclude that all portions of the dorsal striatal functional network are present in the tree pangolin in a manner like that observed in other mammals.

While the dorsal striatal circuitry has long been associated with the control and refinement of motor activity, additional evidence has indicated that these nuclei and circuits are involved in reward and decision making (e.g., Balleine et al., 2007), as well as implicit learning and other memory systems (e.g., McDonald & White, 1994; Devan et al., 2011; Do et al., 2013). Given the broad similarities in cyto-, myelo-, and chemoarchitecture observed in the tree pangolin with that in other mammals, it would be reasonable to conclude that the dorsal striatal circuitry, and the functional attributes of this circuitry in the tree pangolin, are likely to be very similar to that observed in other mammals.

ACKNOWLEDGMENTS

We thank Dr. Elizabeth Ebewele of the Department of Forestry, Federal Ministry of Environment, Nigeria, for her assistance in helping to facilitate the issuance of the CITES permit.This work was supported by funding from the National Research Foundation-Third World Academy of Science African Renaissance Doctoral Fellowship (A. I.), and the South African National Research Foundation (P. R. M.).

DATA AVAILABILITY STATEMENT

Data have not been shared due to this study being based on histological sections.

CONFLICT OF INTEREST

The authors declare no conflicts of interest.

AUTHOR CONTRIBUTION

P. R. M. conceptualized the study. A. I., A. B., M. S. A., and P. R. M. obtained the brains. A. I., A. B., and P. R. M. performed the staining and analysis. A. I. and P. R. M. wrote the manuscript, and the remaining authors contributed to the editing and improvement of the early drafts of the manuscript. All authors had full access to all data in the study and take responsibility for the integrity of the data and the accuracy of the data analysis.

PEER REVIEW

The peer review history for this article is available at https://publons.com/publon/10.1002/cne.25353.

ORCID

Aminu Imam https://orcid.org/0000-0003-2371-3065
Paul R. Manger https://orcid.org/0000-0002-1881-2854

REFERENCES

Abellán, A., Vernier, B., Rétaux, S., & Medina, L. (2010). Similarities and differences in the forebrain expression of *Lhx1* and *Lhx5* between chicken and mouse: Insights for understanding telencephalic development and evolution. *Journal of Comparative Neurology*, *518*, 3512–3528. https://doi.org/10.1002/cne.22410

Abellán, A., Desfilis, E., & Medina, L. (2014). Combinatorial expression of *Lef1*, *Lhx2*, *Lhx5*, *Lhx9*, *Lmo3*, *Lmo4*, and *Prox1* helps to identify comparable subdivisions in the developing hippocampal formation of mouse and chicken. *Frontiers in Neuroanatomy*, *8*, 59. https://doi.org/10.3389/fnana.2014.00059

Adrio, F., Rodriguez-Moldes, I., & Anadon, R. (2011). Distribution of glycine immunoreactivity in the brain of the Siberian sturgeon (*Acipenser baeri*): Comparison with γ-aminobutyric acid. *Journal of Comparative Neurology*, *519*, 1115–1142. https://doi.org/10.1002/cne.22556

Alheid, G. F. (2003). Extended amygdala and basal forebrain. *Annals of the New York Academy of Sciences*, *985*, 185–205. https://doi.org/10.1111/j.1749-6632.2003.tb07082.x

Alonso, A., Trujillo, C. M., & Puelles, L. (2020). Longitudinal developmental analysis of prethalamic eminence derivatives in the chick by mapping of Tbr1 *in situ* expression. *Brain Structure and Function*, *225*, 481–510. https://doi.org/10.1007/s00429-019-02015-3

Balleine, B. W., Delgado, M. R., & Hikosaka, O. (2007). The role of the dorsal striatum in reward and decision-making. *Journal of Neuroscience*, *27*, 8161–8165. https://doi.org/10.1523/JNEUROSCI.1554-07.2007

Brown, J. P., Couillard-Despres, S., Cooper-Kuhn, C. M., Winkler, J., Aigner, L., & Kuhn, H. G. (2003). Transient expression of doublecortin during adult neurogenesis. *Journal of Comparative Neurology*, *467*, 1–10. https://doi.org/10.1002/cne.10874

Bunce, J. G., Zikopoulos, B., Feinberg, M., & Barbas, H. (2013). Parallel prefrontal pathways reach distinct excitatory and inhibitory systems in memory-related rhinal cortices. *Journal of Comparative Neurology*, *521*, 4260–4283. https://doi.org/10.1002/cne.23413

Chen, S. Y., Lu, K. M., Ko, H. A., Huang, T. H., Hao, J. H. J., Yan, Y. T., Chang, S. L. Y., Evans, S. M., & Liu, F. C. (2020). Parcellation of the striatal complex into dorsal and ventral districts. *Proceedings of the National Academy of Science United States of America*, *117*, 7418–7429. https://doi.org/10.1073/pnas.1921007117

Colloby, S. J., Elder, G. J., Rabee, R., O'Brien, J. T., & Taylor, J. P. (2016). Structural grey matter changes in the substantia innominata in Alzheimer's disease and dementia with Lewy bodies: A DARTEL-VBM study. *Geriatric Psychiatry*, *32*, 615–623. https://doi.org/10.1002/gps.4500

Crestani, C. C., Alves, F. H. F., Gomes, F. V., Resstel, L. B. M., Correa, F. M. A., & Herman, J. P. (2013). Mechanisms in the bed nucleus of the stria terminalis involved in control of autonomic and neuroendocrine functions: A review. *Current Neuropharmacology*, *11*, 141–159. https://doi.org/10.2175/1570159X11311020002

de Olmos, J. S., Beltramino, C. A., & Alheid, C. (2004). Amygdala and extended amygdala of the rat: A cytoarchitectonical, fibroarchitectonical, and chemoarchitectonical survey. In G. Paxinos (Ed.), *The Rat Nervous System*, *Third Edition* (pp. 509–603). Amsterdam: Elsevier-Academic Press.

Devan, B. D., Hong, N. S., & McDonald, R. J. (2011). Parallel associative processing in the dorsal striatum: Segregation of stimulus-response and cognitive control subregions. *Neurobiology of Learning and Memory*, *96*, 95–120. https://doi.org/10.1016/j.nlm.2011.06.002

Do, J., Kim, J. I., Bakes, J., Lee, K., & Kaang, B. K. (2013). Functional roles of neurotransmitters and neuromodulators in the dorsal striatum. *Learning & Memory*, *20*, 21–28. https://doi.org/10.1101/lm.025015.111

Dong, H. W., & Swanson, L. W. (2003). Projections from the rhomboid nucleus of the bed nuclei of the stria terminalis: Implications for cerebral hemisphere regulation of ingestive behaviors. *Journal of Comparative Neurology*, *463*, 434–472. https://doi.org/10.1002/cne.10758

Dong, H. W., & Swanson, L. W. (2004). Projections from bed nuclei of the stria terminalis, posterior division: Implications for cerebral hemisphere regulation of defensive and reproductive behaviors. *Journal of Comparative Neurology*, *471*, 396–433. https://doi.org/10.1002/cne.20002

Geula, C., Dunlop, S. R., Ayala, I., Kawles, A. S., Flanagan, M. E., Gefen, T., & Mesulam, M. M. (2021). Basal forebrain cholinergic system in the dementias: Vulnerability, resilience, and resistance. *Journal of Neurochemistry*, *158*, 1394–1411. https://doi.org/10.1111/jnc.15471

Griffin, G. D., Ferri-Kolwicz, S. L., Reyes, B. A. S., van Bockstaele, E. J., & Flanagan-Cato, L. M. (2010). Ovarian hormone-induced reorganization of oxytocin-labeled dendrites and synpases lateral to the hypothalamic ventromedial nucleus in female rats. *Journal of Comparative Neurology*, *518*, 4531–4545. https://doi.org/10.1002/cne.22470

Hirano, A. A., Brandstatter, J. H., Morgans, C. W., & Brecha, N. C. (2011). SNAP25 expression in mammalian retinal horizontal cells. *Journal of Comparative Neurology*, *519*, 972–988. https://doi.org/10.1002/cne.22562

Imam, A., Ajao, M. S., Bhagwandin, A., Ihunwo, A. O., & Manger, P. R. (2017). The brain of the tree pangolin (*Manis tricuspis*). I. General appearance of the central nervous system. *Journal of Comparative Neurology*, *525*, 2571–2582. https://doi.org/10.1002/cne.24222

Imam, A., Bhagwandin, A., Ajao, M. S., Spocter, M. A., Ihunwo, A. O., & Manger, P. R. (2018a). The brain of the tree pangolin (*Manis tricuspis*). II. The olfactory system. *Journal of Comparative Neurology*, *526*, 2548–2569. https://doi.org/10.1002/cne.24510

Imam, A., Bhagwandin, A., Ajao, M. S., Ihunwo, A. O., Fuxe, K., & Manger, P. R. (2018b). Brain of the tree pangolin (*Manis tricuspis*). III. The unusual locus coeruleus complex. *Journal of Comparative Neurology*, *526*, 2570–2584. https://doi.org/10.1002/cne.24519

Imam, A., Bhagwandin, A., Ajao, M. S., Ihunwo, A. O., & Manger, P. R. (2019a). The brain of the tree pangolin (*Manis tricuspis*). IV. The hippocampal formation. *Journal of Comparative Neurology*, *527*, 2393–2412. https://doi.org/10.1002/cne.24519

Imam, A., Bhagwandin, A., Ajao, M. S., & Manger, P. R. (2019b). The brain of the tree pangolin (*Manis tricuspis*). V. The diencephalon and hypothalamus. *Journal of Comparative Neurology*, *527*, 2413–2439. https://doi.org/10.1002/cne.24619

Imam, A., Bhagwandin, A., Ajao, M. S., Spocter, M. A., & Manger, P. R. (2019c). The brain of the tree pangolin (*Manis tricuspis*). V. The brainstem and cerebellum. *Journal of Comparative Neurology*, *527*, 2440–2473. https://doi.org/10.1002/cne.24721

Imam, A., Bhagwandin, A., Ajao, M. S., & Manger, P. R. (2022). The brain of the tree pangolin (*Manis tricuspis*). VII. The amygdaloid body. *Journal of Comparative Neurology*, submitted. https://doi.org/10.1002/cne.25345

Ju, G., & Swanson, L. W. (1989). Studies on the cellular architecture of the bed nuclei of the stria terminalis in the rat: I. Cytoarchitecture. *Journal of Comparative Neurology*, *280*, 587–602. https://doi.org/10.1002/cne.902800409

Kaiser, A., Alexandrova, O., & Grothe, B. (2011). Urocortin-expressing olivocochlear neurons exhibit tonotopic and developmental changes in the auditory brainstem and in the innervation of the cochlea. *Journal of Comparative Neurology*, *519*, 2758–2778. https://doi.org/10.1002/cne.22650

Koulousakis, P., Andrade, P., Visser-Vandewalle, V., & Sesia, T. (2019). The nucleus basalis of Meynert and its role in deep brain stimulation for cognitive disorders: A historical perspective. *Journal of Alzheimer's Disease*, *69*, 905–919. https://doi.org/10.3233/JAD-180133

Lanciego, J. L., Luquin, N., & Obeso, J. A. (2012). Functional neuroanatomy of the basal ganglia. *Cold Spring Harbor Perspectives in Medicine*, *2*, a009621. https://doi.org/10.1101/cshperspect.a009621

Laux, A., Delalande, F., Mouheiche, J., Stuber, D., van Dorsselaer, A., Bianchi, E., Bezard, E., Poisbeau, P., & Goumon, Y. (2012). Localization of endogenous morphine-like compounds in the mouse spinal cord. *Journal of Comparative Neurology*, *520*, 1547–1561. https://doi.org/10.1002/cne.22811

Lebow, M. A., & Chen, A. (2016). Overshadowed by the amygdala: The bed nucleus of the stria terminalis emerges as key to psychiatric disorders. *Molecular Psychiatry*, *21*, 450–463. https://doi.org/10.1038/mp.2016.1

Li, S., & Kiruoac, J. (2008). Projections from the paraventricular nucleus of the thalamus to the forebrain, with special emphasis on the extended amygdala. *Journal of Comparative Neurology*, *506*, 263–287. https://doi.org/10.1002/cne.21502

Liu, A. K. L., & Gentleman, S. M. (2021). Chapter 11 – The diagonal band of Broca in health and disease. In D. F. Swaab, F. Kreier, P. J. Lucassen, A. Salehi, & R. M. Buijs (Eds.), *The Human Hypothalamus: Anterior Region. Handbook of Clinical Neurology, Volume 179* (pp. 175–187). Amsterdam: Elsevier. https://doi.org/10.1016/B978-0-12-819975-6.00009-1

Mai, J. K., & Ashwell, K. W. S. (2004). Chapter 3 – Fetal development of the central nervous system. In G. Paxinos, & J. K. Mai (Eds.), *The Human Nervous System*, *Second Edition* (pp. 95–110). Amsterdam: Elsevier-Academic Press.

Manduca, A., Servadio, M., Damsteegt, R., Campolongo, P., Vanderschuren, L. J., & Trezza, V. (2016). Dopaminergic neurotransmission in the nucleus accumbens modulates social play behaviour in rats. *Neuropsychopharmacology*, *41*, 2215–2223. https://doi.org/10.1038/npp.2016.22

McDonald, R. J., & White, N. M. (1994). Parallel information processing in the water maze: Evidence for independent memory systems

involving dorsal striatum and hippocampus. *Behavioral and Neural Biology*, *61*, 260–270. https://doi.org/10.1016/S0163-1047(05)80009-3

Medina, L., & Abellán, A. (2012). Chapter 7. Subpallial structures. In C. Watson, G. Paxinos, & L. Puelles (Eds.), *The Mouse Nervous System* (pp. 173–220). Oxford: Elsevier Inc. https://doi.org/10.1016/B978-0-12-369497-3.10007-X

Mocellin, P., & Mikulovic, S. (2021). The role of the medial septum-associated networks in controlling locomotion and motivation to move. *Frontiers in Neural Circuits*, *15*, 699798. https://doi.org/10.3389/fn-cir.2021.699798

Murata, K. (2020). Hypothetical roles of the olfactory tubercle in odor-guided eating behavior. *Frontiers in Neural Circuits*, *14*, 577880. https://doi.org/10.3389/fn-cir.2020.577880

Ngwenya, A., Patzke, N., Manger, P. R., & Herculano-Houzel, S. (2016). Continued growth of the central nervous system without mandatory addition of neurons in the Nile crocodile (*Crocodylus niloticus*). *Brain, Behavior and Evolution*, *87*, 19–38. https://doi.org/10.1159/000443201

Patzke, N., Spocter, M. A., Karlsson, K. Æ., Bertelsen, M. F., Haagensen, M., Chawana, R., Streicher, S., Kaswera, C., Gilissen, E., Alagaili, A. N., Mohammed, O. B., Reep, R. L., Bennett, N. C., Siegel, J. M., & Ihunwo, A. O., & Manger, P. R. (2015). In contrast to many other mammals, cetaceans have relatively small hippocampi that appear to lack adult neurogenesis. *Brain Structure and Function*, *220*, 361–383. https://doi.org/10.1007/s00429-013-0660-1

Paxinos, G., Watson, C., Carrive, P., Kirkcaldie, M. T. K., & Ashwell, K. (2009). *Chemoarchitectonic Atlas of the Rat Brain*. Amsterdam: Elsevier.

Pillay, S., Bhagwandin, A., Bertelsen, M. F., Patzke, N., Engler, G., Engel, A. K., & Manger, P. R. (2017). Regional distribution of cholinergicm catecholaminergic, serotonergic and orexinergic neurons in the brain of two carnivore species: The feliform banded mongoose (*Mungos mungo*) and the caniform domestic ferret (*Mustela putorius furo*). *Journal of Chemical Neuroanatomy*, *82*, 12–28. https://doi.org/10.1016/j.jchemneu.2017.04.001

Piskuric, N. A., Vollmer, C., & Nurse, C. A. (2011). Confocal immunofluorescence study of rat aortic body chemoreceptors and associated neurons *in situ* and *in vitro*. *Journal of Comparative Neurology*, *519*, 856–873. https://doi.org/10.1002/cne.22553

Ploeger, G. E., Willemen, A. P. M., & Cools, A. R. (1991). Role of the nucleus accumbens in social memory in rats. *Brain Research Bulletin*, *26*, 23–27. https://doi.org/10.1016/0361-9230(91)90187-O

Radley, J. J., & Johnson, S. B. (2018). Anteroventral bed nuclei of the stria terminalis neurocircuitry: Towards an integration of HPA axis modulation with coping behaviors. *Psychoneuroendocrinology*, *89*, 239–249. https://doi.org/10.1016/j.psyneuen.2017.12.005

Radtke-Schuller, S. (2018). *Cyto- and Myeloarchitectural Brain Atlas of the Ferret (Mustela putorius) in MRI Aided Stereotaxic Coordinates*. Switzerland: Springer International Publishing AG.

Risold, P. Y. (2004). The septal region. In G. Paxinos (Ed.), *The Rat Nervous System*, *Third Edition* (pp. 605–632). Amsterdam: Elsevier-Academic Press.

Risold, P. Y., & Swanson, L. W. (1997). Connections of the rat lateral septal complex. *Brain Research Reviews*, *24*, 115–195. https://doi.org/10.1016/S0165-0173(97)00009-X

Roddy, D. W., Roman, E., Rooney, S., Andrews, S., Farrell, C., Doolin, K., Levins, K. J., Tozzi, L., Tierney, P., Barry, D., Frodl, T., O'Keane, V., & O'Hanlon, E. (2018). Awakening neuropsychiatric research into the stria medullaris: Development of a diffusion-weighted imaging tractography protocol of this key limbi structure. *Frontiers in Neuroanatomy*, *12*, 39. https://doi.org/10.3389/f.nana.2018.00039

Roland, J. J., Stewart, A. L., Janke, K. L., Gielow, M. R., Kostek, J. A., Savage, L. M., Servatius, R. J., & Pang, K. C. H. (2014). Medial septum-diagonal band of Broca (MSDB) GABAergic regulation of hippocampal acetylcholine efflux is dependent on cognitive demands. *Journal of Neuroscience*, *34*, 506–514. https://doi.org/10.1523/JNEUROSCI.2352-13.2014

Salgado, S., & Kaplitt, M. G. (2015). The nucleus accumbens: A comprehensive review. *Stereotactic and Functional Neurosurgery*, *93*, 75–93. https://doi.org/10.1159/000368279

Somerville, L. H., Whalen, P. J., & Kelley, W. M. (2010). Human bed nucleus of the stria terminalis indexes hypervigilant threat monitoring. *Biological Psychiatry*, *68*, 416–424. https://doi.org/10.1016/j.biopsych.2010.04.002

Smith, K. S., Tindell, A. J., Aldridge, J. W., & Berridge, K. C. (2009). Ventral pallidum roles in reward and motivation. *Behavioral Brain Research*, *196*, 155–167. https://doi.org/10.1016/j.bbr.2008.09.038

Sternberger, L. A., & Sternberger, N. H. (1983). Monoclonal antibodies distinguish phosphorylated and nonphosphorylated forms of neurofilaments *in situ*. *Proceedings of the National Academy of Science United States of America*, *80*, 6126–6130. https://doi.org/10.1073/pnas.80.19.6126

Villano, I., Messina, A., Valenzano, A., Moscatelli, F., Esposito, T., Monda, V., Esposito, M., Precenzano, F., Carotenuto, M., Viggiano, A., Chieffi, S., Cibelli, G., Mondam, M., & Messina, G. (2017). Basal forebrain cholinergic system and orexin neurons: Effects on attention. *Frontiers in Behavioral Neuroscience*, *11*, 10. https://doi.org/10.3389/fnbeh.2017.00010

Walker, D. L., Toufexis, D. J., & Davis, M. (2003). Role of the bed nucleus of the stria terminalis versus the amygdala in fear, stress, and anxiety. *European Journal of Pharmacology*, *463*, 199–216. https://doi.org/10.1016/S00014-2999(03)01282-2

Watson, C., Mitchelle, A., & Puelles, L. (2017). A new mammalian brain ontology based on developmental gene expression. In J. H. Kaas (Ed.), *Evolution of Nervous Systems*, 2nd edn. (pp. 53–75). Oxford: Elsevier.

Wirtshafter, H. S., & Wilson, M. A. (2021). Lateral septum as a nexus for mood, motivation, and movement. *Neuroscience & Biobehavioral Reviews*, *126*, 544–559. https://doi.org/10.1016/j.neubiorev.2021.03.029

Wong, P., Gharbawie, O. A., Luethke, L. E., & Kaas, J. H. (2008). Thalamic connections of architectonic subdivisions of temporal cortex in grey squirrels (*Sciurus carolinensis*). *Journal of Comparative Neurology*, *510*, 440–461. https://doi.org/10.1002/cne.21805

Zhou, L., Furuta, T., & Kaneko, T. (2004). Neurokinin B-producing projection neurons in the lateral stripe of the striatum and cell clusters of the accumbens nucleus in the rat. *Journal of Comparative Neurology*, *480*, 143–161. https://doi.org/10.1002/cne.20331

How to cite this article: Imam, A., Bhagwandin, A., Ajao, M. S., & Manger, P. R. (2022). The brain of the tree pangolin (*Manis tricuspis*). VIII. The subpallial telencephalon. *J Comp Neurol*, *530*, 2611–2644. https://doi.org/10.1002/cne.25353